The Role of Energy Deposition Processes in the Understanding of Laser Microprobe Analysis Mechanisms

Akos Vertes
Central Research Institute for Physics of the Hungarian Academy of Sciences

Peter Juhasz
Central Research Institute for Physics of the Hungarian Academy of Sciences

Marc De Wolf
University of Antwerp

Renaat Gijbels
University of Antwerp

Recommended Citation

THE ROLE OF ENERGY DEPOSITION PROCESSES
IN THE UNDERSTANDING OF LASER MICROPROBE ANALYSIS MECHANISMS

Akos Vertes*, Peter Juhasz, Marc De Wolf[+] and Renaat Gijbels[+]

Central Research Institute for Physics of the Hungarian Academy of Sciences,
P.O.Box 49., H-1525 Budapest 114. (Hungary)
[+]Department of Chemistry, University of Antwerp (U.I.A.),
Universiteitsplein 1, B-2610 Wilrijk (Belgium)

Abstract

After emphasizing the role of local energy deposition as a common feature of many microanalytical techniques we focus our attention to laser ionization processes in mass spectrometry of solids. Enhancement of ionization in the case of high power density laser pulses can be rationalized in terms of hydrodynamic equations. The mechanism of shock wave generation and plasma ignition as well as excess energy absorption is demonstrated. Model calculations show that a one component - one dimensional (1C-1D) description can account for such important features of the laser ionization process as energy distribution of the produced ions. The role of classical absorption in the determination of plasma formation threshold is unfolded. Present efforts to relate the results with the fine structure of mass spectra are outlined. Targets are most commonly strongly inhomogeneous in practical microprobing. The induced plasma ignition concept is introduced in order to describe poorly reproducible mass spectra in these situations.

*Address for correspondence:
A. Vertes
Department of Chemistry, University of Antwerp (U.I.A.), Universiteitsplein 1, B-2610 Wilrijk, Belgium
Phone: (32)(3) 828.25.28 /250
Electronic mail: VERTES@BANUIA52.BITNET

Introduction

Local chemical analysis of a sample always includes as a step the microscopic excitation of the target with electromagnetic or particle beams; this step can also be regarded as a local energy deposition. Depending on the characteristics of the exciting beams we can classify the different microprobe techniques. Wavelength, intensity and duration of illumination determine which degree of freedom of the target spot can be excited with electromagnetic waves. According to this, we can distinguish between microfocused X-ray fluorescent analysis, resonant or non resonant multiphoton ionization, laser desorption, laser plasma ionization or simply microscopic spectrophotometry. Similar examples can be mentioned from the field of particle beams. The beams can consist of elementary particles such as electrons, protons, neutrons or of neutral atoms, molecules or their ions.

Further subdivisions can be made according to the detected species which carries the information about the chemical composition of the probed spot. In most of these techniques we can detect both electromagnetic waves and particles. We further confine ourselves to situations in which ions generated in the beam target interaction are detected. Consequently we also exclude such important methods as electron probe X-ray microanalysis (EPXMA), Rutherford backscattering (RBS), particle induced X-ray emission (PIXE), Auger electron spectrometry (AES).

In the forefront of the remaining techniques, we find the two most powerful microprobes: based on laser ionization (LIMS) and the secondary ionization mass spectrometers (SIMS), which achieve the highest sensitivity for elemental and isotopic analysis. Typical commercially available examples of LIMS microprobes are the LAMMA-1000 from Leybold Heraeus and the LIMA 3 from Kratos Analytical. The selection of microprobes is broader in the case of SIMS since the technique has a longer history. Just to name a few: IMS 4f from Cameca, MIQ-156 from ISA Riber, IMA-2A from Hitachi, etc.

Energy deposition and redistribution in the sample as a possible key to the understanding of these methods will be outlined in the first part of the paper. We give

special emphasis to the similarities between the processes involved in SIMS and LIMS techniques.

In the second part we will take a closer look at laser ionization, using a hydrodynamic description in rationalizing a large body of experimental observations available in the field.

The origin of the local energy deposition concept dates back to early investigations of radiation damage in solid materials. A comprehensive review of this subject including the early version of the temperature spike approach was written by Seitz and Koehler, (1956). The basic idea was that the high energy particle entering the target mediates its energy to the neighborhood through a collision cascade. The transferred energy heats up the surrounding of the track making atomic rearrangements possible.

This same idea reappears in the present literature of secondary and laser ionization in many ways, with the main difference that now we concentrate on the removed particles rather than on target damage.

There is another technique, the spark source mass spectrometry (SSMS) which can also be discussed in terms of energy deposition (Ramendik et al. 1987). Although it has never become a tool of local analysis, microscopic analytical capabilities have been demonstrated recently by Swenters et al. (1987), among others. The energy deposition concept has been used for a long time in the explanation of spark source mass spectrometric ion formation (see review by Ramendik et al., 1988).

According to the most probable mechanism in the sparking process, electrons, field emitted from the cathode, hit the surface of the anode depositing part of their kinetic energy gained from the electric field.

The deposited energy determines the basic features of the mass spectra. Part of the energy is devoted to the atomization of the electrode material. This process leads to morphological and chemical surface modifications as described by Verlinden et al. (1985) and by Swenters et al. (1986). Other parts of the deposited energy are used for ionization and for conversion into the kinetic energy of the atomized and/or ionized particles giving rise to ion energies as large as several hundred eV (see Fig. 1).

Ramendik et al. (1981) and Van Puymbroek et al. (1984) emphasized that the different energy distributions of the different ions combined with the limited energy acceptance of the spectrometer result in discrimination effects. Both this and the above mentioned electrode surface modification effect may account for the spread of relative sensitivity factors for different ionic species.

There is a difference of some 20 years between the introduction of the energy deposition concept in SIMS and LIMS in accordance with a similar time difference in the launching and practical use of the two techniques. So, it is most certainly useful to compare the results of both fields, since similarities may lead to benefits in the development of the less advanced LIMS theory. Because of this objective we will give a less detailed review of the

SIMS literature, and will pay attention only to those aspects which can contribute to the understanding of LIMS as well. The reader interested more in SIMS is referred to the excellent book of Benninghoven et al. (1987).

To visualize the most important processes relevant in SIMS and LIMS based microprobes we first briefly describe the steps of local energy deposition in these situations. This part will be followed by the short review of the existing models. Introduction, solution and discussion of our hydrodynamic model can be found afterwards.

Steps of local energy deposition

Before any interaction takes place between the sample and the probing beam the situation is obvious. We have an energetic beam and a solid sample as it is prepared for investigation. After the analysis has been done the situation is simple again. The beam is partly absorbed, reflected or transmitted, the sample is more or less damaged and part of it is emitted in the form of neutral and/or charged particles.

There is a large body of investigations devoted to particle removal, redistribution and implantation in general. These processes acquired some technological significance and their application span from ion sputtering and ion implantation to laser annealing and laser drilling. Particle sputtering or particle ejection, however is not our main interest. It is only a prerequisite of free ion generation, which provides more or less fragmented cloud of the target material.

Since in mass spectrometry only ions can be detected the main task is to determine the nature, quantity and energy of the emerging charged particles. In order to do this we have to investigate what happens between the initial and final situation, namely the beam - target interaction.

For the understanding of this phase let us consider the typical parameters of the primary beams. In laser ionization Q-switched Nd-YAG, ruby and N_2 lasers are customary. Their wavelengths are in the range of $265nm < \lambda < 1060nm$ and pulse durations cover the region $5nsec < t_{pulse} < 50nsec$. Frequency doubling or quadrupling is widely used for shorter wavelengths. According to the delivered power density, Φ_0, the mechanism of ion formation ranges from simple laser desorption to plasma ionization. Usual values are $10^6 W/cm^2 < \Phi_0 < 10^{11} W/cm^2$, or in photon flux $\Phi_0/(h\nu) = 10^{24} - 5 * 10^{29} photons/(cm^2 sec)$.

In secondary ionization the primary ion beam usually consists of Ar^+, O_2^+, O^- or Cs^+. The kinetic energy of those particles is somewhere between 1keV and 20keV. Typical current densities are $10^{-10} A/cm^2 < i < 10^{-3} A/cm^2$, which correspond to ion fluxes in the range $i = 6 * 10^8 - 6 * 10^{15} ions/(cm^2 sec)$. Contrary to laser ionization we use here continuous excitation instead of pulses.

Comparison of dose densities used in the two cases

may be of interest. To carry out an analysis $5*10^{15}-2*10^{22}photons/cm^2$ or $10^{12}-10^{19}ions/cm^2$ are necessary.

In the beam target interaction, part of the energy carried by the beam is mediated to the target. The energy transfer itself is a multistep process.

I
(rel. units)

a

1

2

3

0   100   200   E(eV)

I
(rel.units)
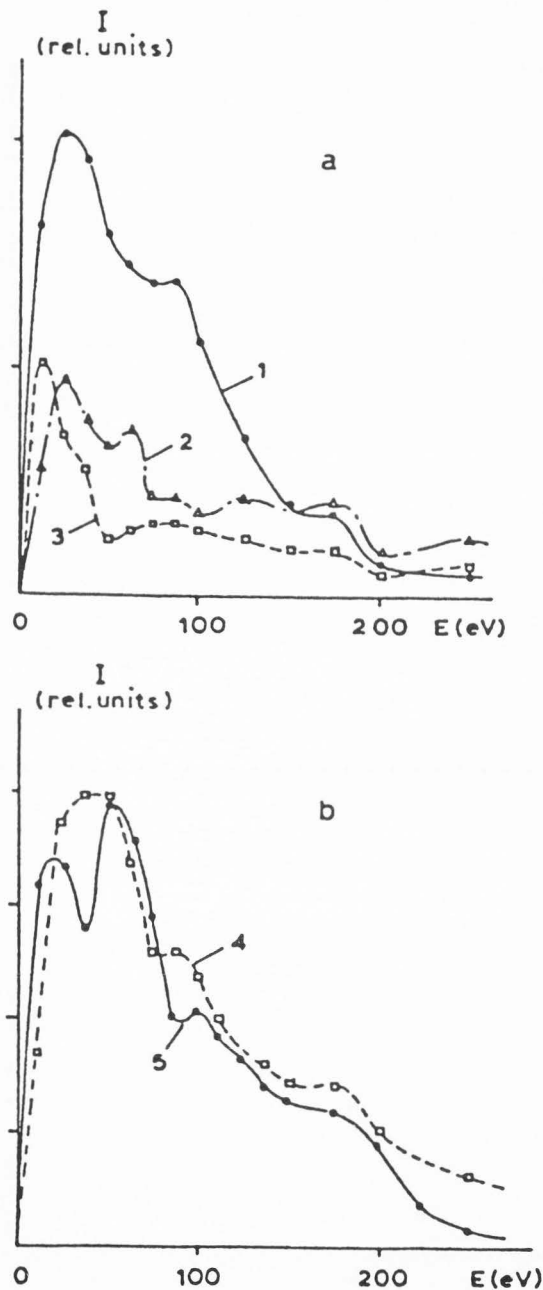
b

4

5

0   100   200   E(eV)

Figure 1. Kinetic energy distribution of ions formed in vacuum spark discharge under usual condition of SSMS. Tantalum probe was used against the International Geological Standard BM-1. The different curves correspond to: a/1-Si^+, a/2-Fe^+, a/3-Ti^+, b/4-O^+, b/5-C^+. The intensity of 2 and 3 on the Figure is increased by a factor of four for easier inspection (taken from the publication of Ramendik et al., 1981.).

Electromagnetic waves can excite some of the internal degrees of freedom of the material. Depending on the spectral range these are lattice or intramolecular vibrations or electronic transitions. Redistribution of this energy leads to heating, erosion, deformation and ionization. Photons, ions, electrons and neutrals are emerging from the interaction region. If the energy of the incoming photons coincides with one of the possible electronic transitions resonant ionization may take place. This is usually not the case unless special efforts are made. On the other hand, as ionization of the material increases due to normal absorption, resonant plasma absorption takes place at a certain critical electron density leading to strong heating of the electron gas. Contrary to resonant ionization this situation usually can be reached since particle density inside the solid is normally above the critical density.

Particle beams according to the widely accepted picture - see for instance Thompson (1981) - transfer their energy to the target by a collision cascade. Individual high energy ions penetrate the surface layers of the sample colliding consecutively with atoms. As a result of the collisions these atoms gain kinetic energy, electronic energy and there is a strong possibility of their ionization too. The deposited energy causes heating, deformation, sputtering of neutrals, photon, electron and ion emission processes.

Due to the usually high fluxes in both laser and ion beams non-equilibrium effects play a vital role during the interaction. For, example if we delivered the same amount of energy in laser ionization to a sample during $5sec$ instead of $5nsec$ we could hardly get any ionization at all.

The emitted ions, in the ideal case, should represent the local composition of the sample both qualitatively and quantitatively. In reality this is far from being true as is well known from the wide variations of the relative sensitivity factors. The outgoing ions can be produced from atoms, molecules and their fragments or clusters in singly or multiple charged forms. These different types are related to specific redistribution processes. Redistribution of the absorbed energy immediately after deposition accounts for the appearance of many of these ions either by fragmentation of atomic aggregates from the surface or by ion molecule or other reactions of the leaving particles. The general situation is schematically explained in Fig. 2.

Models of energy deposition and redistribution

In general, the energy loss of electromagnetic and particle beams can be treated in a quite similar way. In the case of light one usually can define a local absorption coefficient, $\alpha(x,t)$, which determines the local light power density, $\Phi(x,t)$, through an absorption law. The functional form of this law can be expanded in power series of Φ:
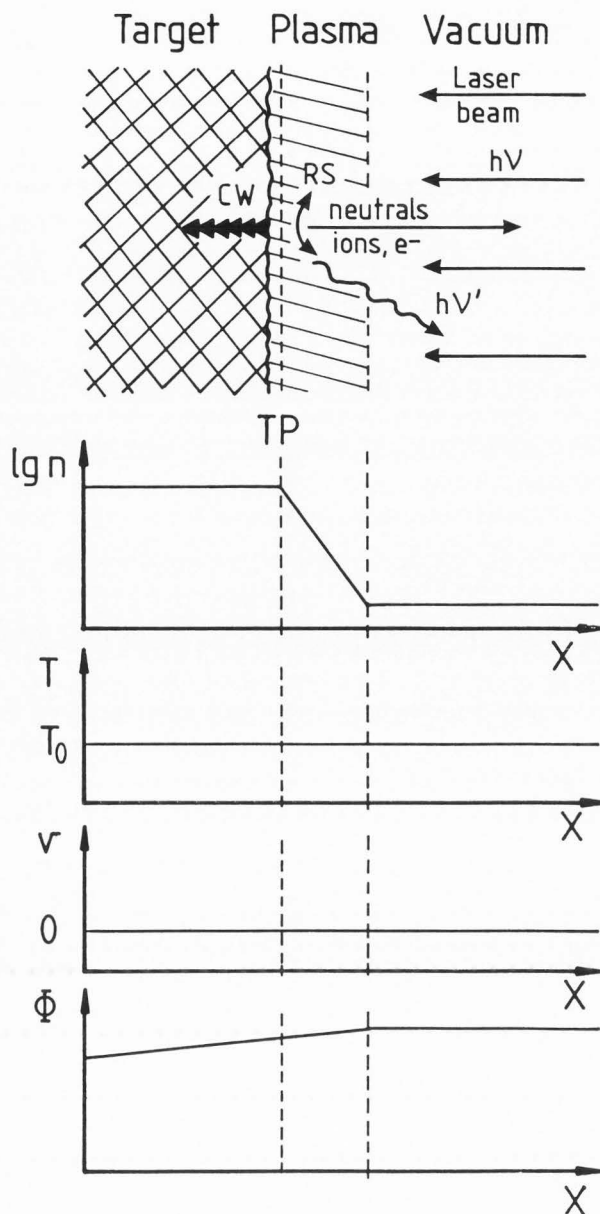
Figure 2. Schematic view of the laser beam - target interaction, together with the initial conditions of our hydrodynamic calculations. We emphasized some elementary processes occurring in the interaction region. Apart from sputtering and plasma formation, compression wave (CW) generation, reactive scattering (RS) of the plasma components and radiative transitions ($h\nu'$) in the plasma are displayed. The initial surface of the solid is called target plane (TP). At the lower part of the Figure initial spatial distributions of particle number density, n, temperature, T, velocity, v and light power density, Φ are shown.

$$\frac{\partial \Phi(x,t)}{\partial x} = -\alpha(x,t)\Phi(x,t) - \beta(x,t)\Phi^2(x,t) + ..., \quad (1)$$

where $\beta(x,t)$ is the first nonlinear coefficient. At normal light intensities only the linear term is important and the absorption law has the form:

$$\Phi(x,t) = \Phi_0 exp\left[-\int_x^\infty \alpha(x',t)dx'\right], \quad (2)$$

where the light propagating along the x axis has initial intensity, Φ_0.

Since non-linearity is usually preceded by evaporation and strong ionization of the material we may estimate its relevance on the basis of non-linear plasma absorption. Non-linear absorption becomes only important if the oscillation energy of the electrons in the plasma, E_{osc}, is comparable to the thermal energy, kT. Using the estimation of E_{osc} (Hora, 1979, p. 72):

$$E_{osc} = \frac{\Phi_0}{2cn_{cr}}, \quad (3)$$

so the laser intensity where non-linear effects start to play a role is:

$$\Phi_0^{thr} = 2ckTn_{cr}. \quad (4)$$

Here n_{cr} is the critical electron density leading to resonant plasma absorption:

$$n_{cr} = \frac{m_e\omega^2}{4\pi e_0^2}. \quad (5)$$

In the case of a ruby laser evaluating Eq. (4) provides: $\Phi_0^{thr} \; (W/cm^2) = 2.5 * 10^9 \; T \; (K)$. To achieve some ionization at least $1000K$ is necessary, therefore the non-linear effects turn on at $\Phi_0^{thr} = 2.5*10^{12} \; W/cm^2$. This is well beyond the interesting region for laser ionization.

Energy loss of particle beams can be treated with the so called nuclear and electronic stopping power of the target, S_n and S_e:

$$\frac{d E}{d x} = -n_a\big(S_n(E) + S_e(E)\big), \quad (6)$$

where n_a denotes the number density of atoms in the target. The functions $S_n(E)$ and $S_e(E)$ are related to the scattering cross sections of target atoms and are subject of laborious calculations. They are expressed in the form of power functions of fractional order (Benninghoven et al., 1987, p. 20-31). It is worthwhile to mention that contrary to laser ionization, secondary ionization is based on strongly non-linear energy deposition processes.

After identifying the amount of energy loss in the

beam we would like to know the fate of the deposited energy in the target. There are numerous different investigations concerning the members of a very complex family of elementary events during the energy redistribution process. We focus our attention only on the approaches which are relevant to microprobe techniques.

Two limiting cases can be separated in both methods. If gentle excitation is used the system doesn't deviate very much from equilibrium and thermodynamic control of the events can be observed. At low energy particle bombardment and at low laser power densities the generated ions will exhibit Maxwellian kinetic energy distribution (Van Der Peyl et al. 1984, Schäfer and Hess, 1985).

In the other limit of extremely severe excitation where strong non-equilibrium processes arise, the control is rather kinetic. As a consequence new mechanisms of ion formation are commonly considered. It is well known, for example, that enhancement of particle yields in the case of high mass and/or high energy primary particles (Ahmad et al. 1980) and high power density light pulses (Conzemius and Capellen 1980) is found. One of the interesting challenges in the field of secondary and laser ionization is undoubtedly the explanation of these effects.

The kinetic energy spectrum of the generated ions in the case of intense excitation also shows remarkable irregularities. Strongly non-Maxwellian behavior

Figure 3. Energy spectra of Si^+ for Xe^+ impact at normal incidence at three different xenon energies. The dashed line corresponds to 10keV Xe_2^+ bombardment. (Figure is from Wittmaack, 1979)

is demonstrated in Fig. 3 for SIMS and in Fig. 5 for LIMS. In the second case the high power density laser pulse induces ion production and the ion kinetic energy distribution exhibits a strong peak in the $100eV$ region. Similar observations for ions, just as for neutrals (Ahmad et al. 1980, Husinsky et al. 1980, Mauney and Adams, 1984, Michiels et al. 1984) draw increasing attention to alternative descriptions capable of predicting these features.

In order to see the possibilities for the general description of laser ionization capable of handling non-Maxwellian ion generation let us have an overview of the existing models having this objective in mind. Three separate classes of the previous models can be distinguished depending on the level of description. The phenomenological, the kinetic and the molecular levels can be clearly separated, although mixing of the levels in one model is also quite frequent. It is necessary to emphasize that this classification is based on differences in the machinery used to describe the processes rather than on differences in the mechanisms investigated.

Phenomenological models

The so called phenomenological models are mostly used in the early stage of investigation since no microscopic knowledge of the processes involved is necessary. In fact the earliest models based on the *spike concept* belong to this group.

The idea is that an energetic beam causes a strong excitation of the target localized in space and time. This excitation can be vigorous heating, permanent displacement of particles, elastic deformation, ionization or any combination of these. Afterwards the excitation spreads radially from the point of generation and this process can be described with the radial form of conservation laws. The energy density, $e_{ini}(\underline{r})$, deposited initially spreads in the target according to:

$$\frac{\partial e}{\partial t} = \nabla \kappa \nabla e, \qquad (7)$$

where $\kappa(e)$ is the thermal conduction coefficient of the material, usually a nonlinear function of the energy density. At every point which reaches the necessary energy density ions are generated and their yield can be calculated using the absolute rate theory of Eyring (Glasstone et al., 1941) for example.

The conventional form of the spike theory deals only with conductive energy transport. This is quite adequate in the case of low energy ion bombardment or low intensity laser desorption. According to the arguments of Sanders (1980), based on spike theory, 6 keV Xe^+ bombardment of Au and RbBr targets doesn't lead to the development of shock waves since coherent motion in the collision cascade is absent.

The *hydrodynamic models* focus on the transport of particle momentum and energy as a continuum during and following energy deposition. Their machinery is
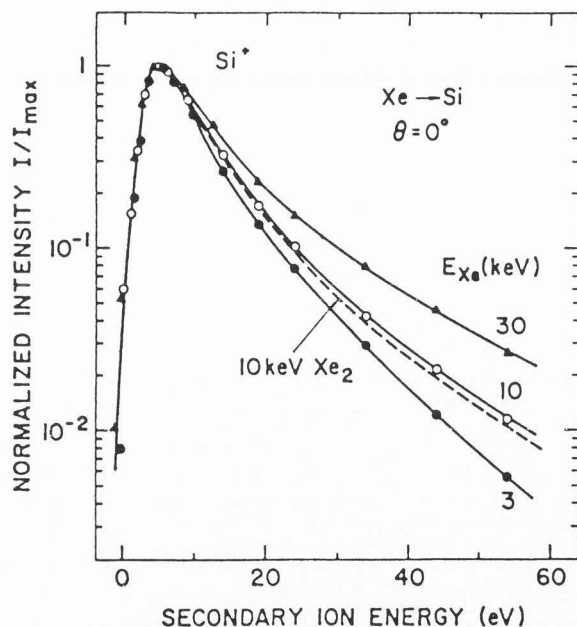
based on conservation laws of these quantities in more or less general form. However, the necessary transport coefficients are usually derived from statistical theories. Since plasma formation in the medium and high incoming flux regions is confirmed, in these cases the transport theory of Spitzer (1962) is widely applied. Details of the hydrodynamic approach will be outlined in below. Here we mention only that hydrodynamic models are well suited for handling strongly non-equilibrium cases.

The best known and most widely used theory of all is the *local thermodynamic equilibrium or LTE theory*. Although it is deliberately used in both SIMS and LIMS (Andersen 1975, Newbury 1980, Castaing and Slodzian, 1981, Odelius et al. 1985, Fürstenau 1981, Haas et al. 1981, Eloy 1985, 1986) for the estimation of ion production its popularity is probably more due to the ease of handling than to coherent arguments. A rigorous description of the model was given by Drawin (1971).

The idea is that from the point of view of ion generation complete thermodynamic equilibrium is reached after the interaction. The only exception is the equilibrium of the target with the perturbing species. Even if we forget about the demonstratedly non-Maxwellian energy distribution of the generated ions (see for instance Benninghoven et al. (1987) for SIMS or Tallents (1980, 1981), Mauney and Adams (1984) and Michiels et al. (1984) for LIMS) the concept contains controversy in itself: extreme non-equilibrium situations are described by an equilibrium theory.

The general law of chemical equilibrium for reactions of the type:

$$AB \rightleftharpoons A + B, \qquad (8)$$
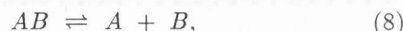
with the net energy change, E_{AB}, can be written in the form:

$$\frac{n_A n_B}{n_{AB}} =$$

$$= \frac{Q_A Q_B}{Q_{AB}} \left(\frac{m_A m_B}{m_A + m_B} \right)^{3/2} \frac{(2\pi kT)^{3/2}}{h^3} exp\left(-\frac{E_{AB}}{kT} \right). \qquad (9)$$

where n_A, n_B, n_{AB} denote the number densities of species A, B, and AB. Q_A, Q_B, Q_{AB} and m_A, m_B, m_{AB} are the corresponding internal partition functions and particle masses respectively.

In the case of ionization processes this formula is simplified to the Saha - Eggert equation and solved in order to provide ionic yields. In many cases E_{AB} is simply identified as atomic or molecular ionization potential, I_p, although more realistic ionization values can be obtained if collective effects in the plasma are taken into account (Drawin, 1971, p. 94-95):

$$E_{AB} = I_p - \frac{e_0^2}{\lambda_D}, \qquad (10)$$

where e_0 is electron charge and λ_D is the Debye screening length:

$$\lambda_D = \left(\frac{kT}{4\pi n_e e_0^2} \right)^{1/2}. \qquad (11)$$

Here λ_D depends on n_e the electron density.

Similarities of the mass spectra obtained by SIMS, fast atom bombardment (FAB), heavy ion induced desorption (HIID), ^{252}Cf fission fragment induced desorption (FIID), infrared and ultraviolet LIMS led Krueger (1983) to the idea of relating their main features to energy deposition and redistribution processes. He established a theoretical model utilizing a *non-equilibrium statistical description* of the phase transition processes, thought to be the common denominator in all these analytical methods. Although the approach is very general and the method is elegant, the large number of unknown parameters makes it difficult to apply the model in real situations.

Another model is based on the *space charge limited current (SCL) theory*. The basic idea is that charge extraction from a plasma cloud in an electric field is limited by the stationary equilibrium between the external field and the internal field generated by the displacement of electron and ion clouds. The extent of this displacement is in the order of λ_D and the current density, j_{SCL}, which can be extracted from the cloud is limited to:

$$j_{SCL} = \frac{1}{9\pi} \left(\frac{2e_0}{m_i} \right)^{1/2} U_a^{3/2} d^{-2}, \qquad (12)$$

where U_a is the extracting potential difference acting on a distance d (see for instance Wilson and Brewer, 1973). So far the application of this theory has been limited to the description of low power density laser ionization (Van der Peyl et al., 1984).

Kinetic models

In situations where individual events governing the distribution of position and velocity of the particles cannot be neglected the phenomenological equations have to be replaced by the Boltzmann type equations (Sigmund, 1969):

$$\frac{\partial f(E,r)}{\partial r} =$$

$$= n \int [f(E,r) - f(E - \Delta E), r)] + n S_e(E) \frac{\partial f(E,r)}{\partial E}, \qquad (13)$$

where $f(E,r)$ is the probability distribution of the primary ion pathlength in the solid, r, at E initial kinetic energy. Typically non-equilibrium processes are treated with this approach.

Individual transitions certainly govern the events in ion bombardment experiments as can be expected from the relatively low incoming flux of ions. Since the basic work of Sigmund (1969) sputtering of solids by ion beams is handled by this formalism quite successfully. He describes the energy transfer to the particles of the target by the concept of *collision cascades*. A cascade is a sequence of mainly elastic collisions between the energetic particles and the atoms of the target.

Sigmund's theory is successful in many applications ranging from ion sputtering through secondary ionization to ion implantation. It is also worked out for different types of targets, such as amorphous and polycrystalline solids and single crystals. As one of the results of the theory it was possible to calculate the spatial distribution of deposited energy and relate it to the quantity of recoiling atoms and to the low energy part of their kinetic energy spectrum in the case of high primary energy particles. Littmark and Sigmund, (1975) extended the energy deposition concept to the deposition of another conserving quantity: the deposition of momentum and calculated the mean velocity of the secondary particles.

The frontiers of the cascade theory are marked by the non-linear collision cascade regime and by the extreme difficulties in the case of complex molecular targets (Kidwell et al. 1987). A cascade is called linear when the density of recoil atoms is sufficiently low to take the events in two different cascades independent. If this condition is not fulfilled the solution of Eq. (13) raises enormous problems and the spike approach is more adequate (Sigmund 1984).

In the case of more and more interesting complex molecular targets the problem is that the conventional formalism of the cascade theory is based on the motion of individual atoms. Although generalization of the model for simple two- or three-atom molecular ion formation was also possible (Gerhard 1975) more complex targets are still not within its scope.

In the case of several molecular samples the gas collision model (Sunner et al. 1986,1988) gives satisfactory results. It is based on the kinetic description of ion-molecule reactions in the dense plasma and capable of predicting secondary ion currents in FAB experiments. This theory is a non-equilibrium complement of the LTE model and in the long residence time limit its results should converge to LTE results.

Recently Johnson (1987) applied the energy deposition concept in the description of ionization spectra of large organic molecules by high energy ions. He addressed the problem of ion generation from organic targets by high energy ions having energies in the order of MeV. In his model the deposited energy partly expands the solid and partly causes permanent bond ruptures leading to fragment ion formation.

Kinetic modeling of events in laser ionization has not been applied so far. Comparison of the incoming fluxes in SIMS and LIMS (see above) explains why: the photon flux is about 14 orders of magnitude higher than the bombarding ion flux, therefore tracing individual absorption events seems hopeless.

Molecular models

In the description of particle beam target interaction it is getting more and more widespread to treat the problem with computer simulation of a large number of scattering events. Here again, the number of elementary events in the case of laser ionization is many orders of magnitude higher. So, it is not promising to carry out similar investigations at the present state of the computer art. Still there are interesting aspects of these simulations worth mentioning in the context of energy deposition.

In the common form of these Monte Carlo simulations, the incoming particle is supposed to travel along a straight line until a collision changes its direction. The energy loss of this particle and consequently the energy transfer to the target is calculated in two parts. At the elastic collisions, the ion transfers energy to the nucleus of its colliding counterpart and between the elastic events inelastic encounters take place with the surrounding electrons.

Primary particle and recoil atom trajectories can be traced, even visualized on the computer display until they completely lose their kinetic energy inducing secondary processes accompanied by the redistribution of the deposited energy. There exists a broad selection of Monte Carlo codes with a wide variety of purposes and special handling of the problem. (The different programs are sometimes identified by acronyms: MARLOWE, Robinson and Torrens, (1974), TRIM, Biersack and Haggmark, (1980), COSIPO, Hautala 1984.)

It is possible with these programs to calculate the spatial distribution of deposited energy related to nuclear and electronic processes, although mainly for simple atomic particles having no internal structure or degrees of freedom. For example, detailed investigations were carried out to determine the dependence of the sputtering yield on the surface deposited energy (Thompson and Johar, 1980). More complex targets are treated by substituting an artificial "effective" solid of simple character instead of the original (Whitlow et al. 1987).

Unlike in laser ionization, under SIMS conditions the incoming particle flux frequently makes it possible to separate the effect of individual cascades. Therefore, the target atoms are in their normal state prior to the interaction with a primary particle or with its recoil atom. Comparing the photon and particle fluxes given above, this is obviously far from true in LIMS. Most probably this basic difference has made it impossible to use Monte Carlo simulations in laser ionization studies and will remain an obstacle for some time.

Hydrodynamic description of target behavior
at laser ionization

Former hydrodynamic investigations of laser light interaction with solid targets focused on nuclear fusion ignition (Caruso and Gratton, 1968, Mulser 1970, 1971; Hora 1979) and construction of heavy ion sources (Yasuda and Sekiguchi, 1979). On the basis of these investigations the main factors governing ion formation turned out to be: the frequency, ν, the time and space distribution of the power density of the laser light, $\Phi_0(\underline{r}, t)$, and optical, thermal and mechanical properties of the target as a function of temperature and pressure. As expected the power density domain of these studies is higher - above $10^{11} W/cm^2$ - than the region of our interest. Still for the benefit of laser ionization studies the machinery of these calculations can be adapted to the situations more interesting to us.

To test these theories and considerations we have to compare them with experimental evidence. Among the most powerful tools of plasma diagnostics - and it is certainly the most important from the point of view of ion sources - there is the measurement of ion kinetic energy distributions. So far, there have been two main types of experiments: one type is based on some kind of energy discriminator like the ion reflector or electrostatic sector (Dinger et al. 1980, Chowdhury et al. 1980, Siegel and Vasile, 1981, Goto et al. 1982, Van Der Peyl et al. 1983, 1984, Mauney and Adams, 1984, Michiels et al. 1984). The other type is based on the simple time of flight principle or on its combination with the retarding potential method (Demtröder and Jantz, 1970, Tabet and Cotter, 1983, Tsong 1986, Vertes et al. 1988).

To summarize the results of these experiments we distinguish between low power density laser desorption and high power density laser plasma ionization. At low power densities only slight fragmentation was observed and the ions produced usually had less then $5eV$ kinetic energy. The distributions could be approximated by Maxwellians (Van Der Peyl et al. 1984, Schäfer and Hess, 1985). A typical example is shown in Fig. 4.

At high power densities the fragmentation becomes more complete leading finally to atomic ions or at even higher laser power multiple charged ions. The kinetic energy spectrum extends over several hundred eV and its width varies with laser power density (see Fig. 5). An interesting feature of the very high power density case is the forward shift of the maximum of the distributions with an increasing charge of the ions.

One of the early ideas was to explain the existence of this shift on the basis of internal electric fields. If electrons and ions have the same temperature the electrons, because of their smaller mass, have higher velocity and escape from the ions. The ions left behind experience an electric field generated by the charge separation and gain momentum according to their charge (Mulser, 1970). It has been shown, however, that this mechanism
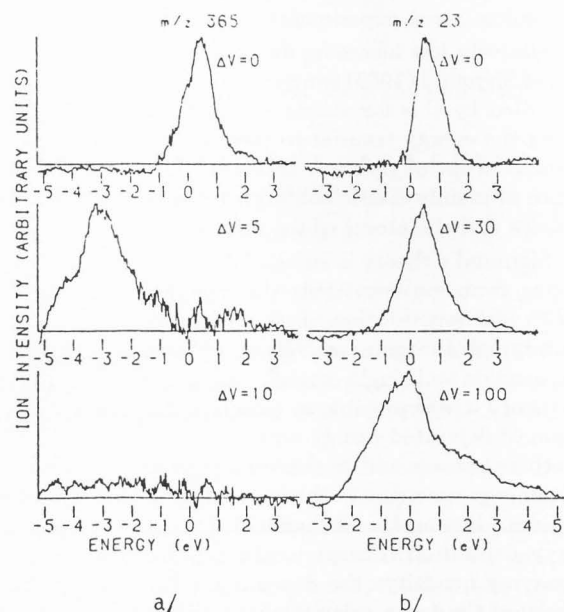

Figure 4. Kinetic energy distribution of a/ $[sucrose + Na]^+$ and b/ Na^+ ions produced under laser desorption conditions (CO_2 laser, $10^7 W/cm^2$). The ΔV values are the extraction voltages in volts. (Published by Van der Peyl et al., 1984.)

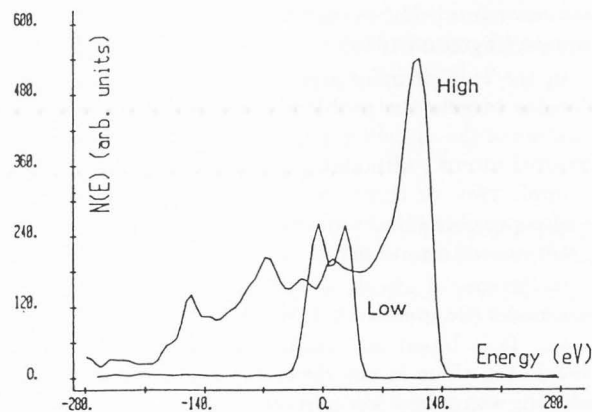Figure 5. Measured kinetic energy distribution of C_2^+ ions at low ($10^6 W/cm^2$) and at high ($10^{10} W/cm^2$) ruby laser power densities (Vertes et al., 1988).

alone cannot account for the total amount of the shift (Mulser, 1971).

Another enormous set of observations is related to the practice of LIMS itself. There are more or less well established empirical rules on the appearance of LIMS spectra, which are their frequently reappearing features. Very good compilations of these rules are available (Hillenkamp 1983,1985, Heinen 1981). Here we list some of

them: the absence of ions with charges larger than one at usual power densities, the non-Maxwellian kinetic energy distributions, the presence of negative ions and frequently abundant cluster ions (Hahn et al. 1986, de Vries 1987, LaiHing et al. 1987, Trevor et al. 1987) just to mention the simplest guiding principles.

In our present effort we will not try to introduce a model which accounts for all these observations. Only the case of a single element target can be considered at this level, and even this simple situation requires numerous approximations.

The model: 1C-1D

It is a bitter but unavoidable step to confine the description as much as possible in order to simplify its solution. On the basis of preliminary trials and previous hydrodynamic calculations we can set up a simple model still anticipating useful results. We started from the general transport theory of a plasma (Braginskii 1965, Sack and Schamel 1987) and tailored the general equations to a form fitting best to our special problem.

Neglecting transport processes perpendicular to the axis of the laser light and considering that on the scale of the spot size the target is flat, one may replace the three dimensional equations with their one dimensional counterparts (1D). Provided, furthermore, that the effect of viscosity and heat conduction can be neglected i. e., the dissipated and conducted energy is insignificant, we abandon the appropriate terms from the equations. Justification of this step can be found from Mulser (1970).

A more drastic simplification seems to be the so called one component (1C) assumption. Since in a plasma the energy of the light is coupled to the target through the electron gas, an enormous difference between the electron and ion temperatures is expected. It is the relaxation time of energy exchange between electrons and ions compared to the time scale of the calculations which justifies the use of a one component model for the description of so many different species.

Preliminary calculations with a two component model taught us that equilibrium of electron and ion temperatures is reached in a very early stage of the calculations especially in the more dense region of the plasma. The energy transfer between the components is a function of the average elapsed time between two collisions, the electron - ion collision time, τ_{ei}:

$$\tau_{ei}^{-1} = \frac{4\sqrt{2\pi}e_0^4 Z^2 n_i ln\Lambda}{3\sqrt{m_e}(kT_e)^{3/2}}. \qquad (14)$$

Here $ln\Lambda$ is the Coulomb logarithm and determined by:

$$\Lambda = \frac{3}{2Ze^3}\left(\frac{k^3 T^3}{\pi n_e}\right)^{1/2}. \qquad (15)$$

Z denotes the charge of the ions. The value of $ln\Lambda$ accounts for the effect of Coulomb interaction in the

electron-ion scattering process. We may extract further evidence about the validity of the 1C model later by inspecting the calculated collision time profiles.

Moreover, according to the extremely different velocity of the electrons and ions, their number density at a certain position may differ significantly. As a measure of the length scale of these deviations the Debye length can serve as a very good estimate since the Coulomb force will try to compensate extreme charge separations (see Eq. (11)). We will calculate Debye length profiles across a solid target - expanding plasma - vacuum interface in order to justify this assumption.

Using all these simplifications we can write the conservation of mass, momentum and energy in the divergence form and in a reference frame at rest (Eulerian system) as follows:

$$\frac{\partial \underline{R}}{\partial t} = -\frac{\partial \underline{F}}{\partial x}, \qquad (16)$$

where the vector $\underline{R}$ stands for the generalized densities:

$$\underline{R} = [\rho, \rho v, \rho(e + v^2/2)]. \qquad (17)$$

The components are the mass, momentum and energy densities expressed with velocity, v, and internal energy density, ρe. The vector $\underline{F}$ denotes the generalized fluxes composed of the mass, momentum and energy fluxes:

$$\underline{F} = [\rho v, p + \rho v^2, \rho v(e + p/\rho + v^2/2) - \Phi], \qquad (18)$$

where p denotes the pressure. In order to cope with the light absorption problem we had to extend the energy flux with light power density, Φ. The density, energy and velocity variables are extremely steep functions of space and time. The equations of conservation in Eq. (16) have to be complemented by the equation of state relating pressure to density and energy:

$$p = f(\rho, e, \eta). \qquad (19)$$

where η is the degree of ionization: $\eta = n_i/n_{total}$. Considering the ideal gas law, Eq. (19) has the well known form:

$$p = (1 + \eta)\rho kT/m. \qquad (20)$$

The internal energy density is related to the state variables:

$$\rho e = \frac{\rho}{m}\left[\frac{3}{2}(1 + \eta)kT + \eta I_p\right], \qquad (21)$$

To determine the degree of ionization the Saha - Eggert equation was used with the customary simplifi-

cations:

$$\frac{\eta^2}{1-\eta} = \frac{m}{\rho}\left(\frac{2\pi k T m_e}{h^2}\right)^{3/2} exp\left(-\frac{I_p}{kT}\right). \quad (22)$$

where I_p is the ionization potential.

The linear light absorption coefficient, $\alpha(x,t)$, of Eq. (1) is built up of two terms. The first accounts for the normal absorption of the solid, α_0, without ionization and the second takes into account the absorption of the plasma cloud, α_{pl}, (Dawson et al., 1969):

$$\alpha(x,t) = \alpha_0(x,t) + \alpha_{pl}(x,t), \quad (23)$$

$$\alpha_{pl} = \frac{2\omega}{c} Im \sqrt{1 - \frac{\omega_p^2}{\omega^2\left(1+\frac{i}{\tau_{ei}\omega}\right)}}. \quad (24)$$

The plasma absorption in high optical-density gradient situations has a strong resonance at the critical density and the light cannot penetrate into the higher density regions because light which is not absorbed will be totally reflected.

Eqs. (2),(16-18) and (20-24) with the given initial and boundary conditions (see Fig. (2)) form a complete problem which can be solved only numerically.

Methods of calculation

For decades hydrodynamics has been recognized as one of the most well-studied branches of computational physics and numerical mathematics. To pick from the almost uncountable number of existing numerical approximations the most proper one, i. e., that which gives the closest description of the real physical situation, is a crucial point of modeling. Because of the non-linearity of the equations of hydrodynamics an improperly chosen numerical scheme does not yield even a rude approximate solution.

In our case, the physical situation can be delineated as follows. Two phases are present in the ionization source: the solid target consisting of the material to be analyzed and vacuum. As the laser pulse impinges onto the target vigorous heating and subsequent expansion of the partly ionized material starts. In the initial conditions a large discontinuity already is present that will evolve into hydrodynamic anomalies: shock waves, rarefaction waves and contact discontinuities (these will be characterized later).

Thus we had to choose numerical techniques which are intended specially for the treatment of these anomalies. The most frequently employed method adds artificial dissipative terms to the equations of fluid dynamics which can lead to the decay of possible shock waves. This method was introduced by von Neumann and Richt-

myer (1950) and is also known as the artificial viscosity method. More recently several sophisticated methods have been developed to model shock tubes (Vatsya, 1987). The method we have preferred was first described by Godunov (1959) and offers a clear physical interpretation.

Godunov's first scheme

Breakdown of discontinuities depicted in Fig. 6. is an analytically soluble problem for gas expansion in a tube. Godunov's first scheme makes use just of this analytic solution for the finite difference approximation to the solution of the equations of hydrodynamics.
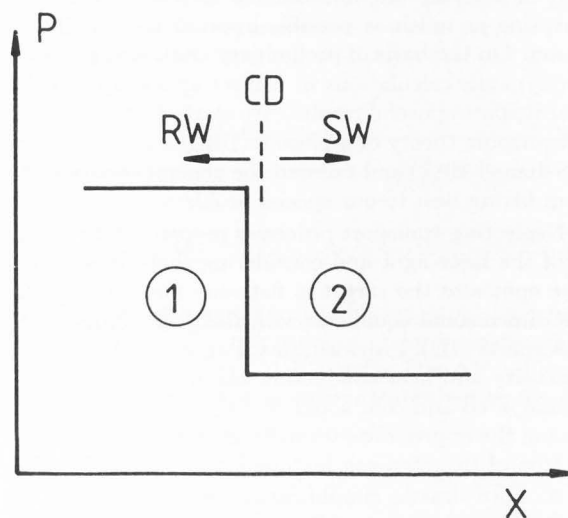

Figure 6. Breakdown of an infinitesimal discontinuity in a pressure vs. position profile. A shock wave (SW) will propagate to the right, a rarefaction wave (RW) to the left and they are separated by a contact discontinuity (CD). Its propagation direction is still not defined by the pressure profile.

In the finite difference approximation the profiles of hydrodynamic quantities at different time levels are represented on a grid. Once these profiles are given at an instant, than at the next time level, advanced by Δt, they can be determined by means of the finite difference form of Eq. (16).

It is clear that the discretized profiles can be perceived as the superposition of step functions similar to the discontinuity shown in Fig. 6. Godunov's idea was to utilize exact formulae for the evolution of these discontinuities arising from the discretization of large gradients. Of course, if during the evolution of the system real shock waves emerge, the algorithm will treat them properly.

The finite difference approximation of Eq. (16) is written as:

$$\frac{R_{j+1/2}^{n+1} - R_{j+1/2}^{n}}{\Delta t} = -\frac{F_{j+1}^{n+1/2} - F_{j}^{n+1/2}}{\Delta x}. \quad (25)$$

Here the upper index specifies the time levels, for instance n corresponds to $t = t_0 + n\Delta t$, the lower index specifies space points, for instance j means $x = x_0 + j\Delta x$.

Starting from the initial conditions (see lower part of Fig. 2.) the generalized density profiles could be calculated at time $n = 0$. Using the implicit breakdown formula of the Godunov scheme (Holt, 1977, p. 33-38) the generalized fluxes were determined at time $n + 1/2$. With the finite difference scheme Eq. (25) we calculated the advanced values of the generalized densities and than the whole procedure was repeated until reaching the final time stage. In every cycle forward and backward transformation of variables has been necessary since the Godunov scheme was based on p, v and ρ while the difference scheme was constructed of generalized quantities.

Determination of temperature and degree of ionization from energy density and pressure required solution of the set of strongly non-linear Eqs. (21) and (22) which was done by the nested interval method.

Details of the calculation and algorithm will be published in a separate paper (in preparation).

Realization

Most common codes of the finite difference schemes use a reference frame with fixed Δx and Δt values. Their choice is governed by the dimensions of the investigated system and the stability condition of the applied scheme. It is easy to see that the presence of the solid - vacuum boundary causes difficulties. Due to the presence of this interface the discretization of the generalized densities leads to extreme differences between neighboring points amounting up to several orders of magnitude. Diminishing the stepsize may help to decrease the drop but it also leads to an enormous increase in the total number of grid points.

The application of adaptive grids can circumvent this difficulty. Initially Δx and Δt were fixed at very small values (on the $10^{-9}m$ and $10^{-13}sec$ scale). The left half of the grid was covered by solid phase values the right half with 'experimental' vacuum values corresponding to about $10^{-6}mbar$ pressure. As the expansion reached the right boundary Δx and Δt were doubled so that their ratio remained the same. After averaging for every neighboring couple of points we could contract the grid to half of its number of meshpoints and the remaining free points were filled with solid and vacuum values on the appropriate sides. Expansion of the plasma could proceed on a larger scale.

This method also had two more advantages. At each moment of the integration we had a complete representation of the profiles in the sense that our field of view zoomed together with the spreading effect of the expan-sion. So the whole region which is influenced by the radiation (in axial sense) has always been covered by the calculation. The other advantage was the diminishing effect of the boundary conditions. Whenever boundary conditions started to play an important role - i.e., when fluxes on the boundaries deviated from zero - with the zooming the boundary points became internal. This is important since in the real experiments the target is usually infinitely large compared to the size of the interaction region.

Calculations were carried out on a VAX 11/780 computer, typically consuming 60 min CPU time for tracing 100 point grids for up to 50 nsec laser heating.

Results and Discussion

We have made model calculations on the ruby laser semi-infinite target interaction at perpendicular incidence angle. Time development of the laser pulse was approximated by a step function. Formation of $M/Z = 24$ $a.m.u.$ ions was investigated at different laser power densities. The laser power was coupled to the target by conventional light absorption where the absorption coefficient is proportional to the number density of the neutrals, n_n, in the form: $\alpha_0 = 10^{-19}n_n(cm^{-3})$. This choice was made arbitrarily so that the absorption coefficient in the solid would reach $\alpha_0 = 10^3 cm^{-1}$. The actual value of this parameter played an important role in the calculations since it directly determined the amount of deposited energy in the first part of the laser pulse. The total absorption coefficient had another component, the absorption of the plasma. α_{pl} is a resonance type function of the number density of electrons showing a sharp increase at the critical density (see Eq. (24)). Since every solid has some residual ionization the linear plasma absorption coefficient, α_{pl}, had a finite positive value even in the solid. The residual degree of ionization was taken equal to 10^{-3}. Its value had no significance on the calculations, since the energy deposition was much more effective through the normal absorption in the early phase of the interaction.

Ignition or warming?

It is important to realize in laser ionization studies that there are two possible regimes depending on the applied light power density. At $10^5 - 10^7 W/cm^2$ mild fragmentation takes place (Day et al. 1981), if any. The ions have a Maxwellian kinetic energy distribution with FWHM usually less than $1eV$. In the range $10^8 - 10^{11}W/cm^2$ real plasma absorption is observed. It is accompanied with heavy fragmentation and the resulting ions exhibit energy distributions extending beyond $10eV$.

Our calculations could reproduce part of these features. Light exposure in the runs was continued up to $50nsec$. In the case of low power density ($\Phi_0 = 10^7 W/cm^2$, see Fig.7) even at the end of the period the plasma absorption was negligible compared to normal absorption. No additional ionization appeared and
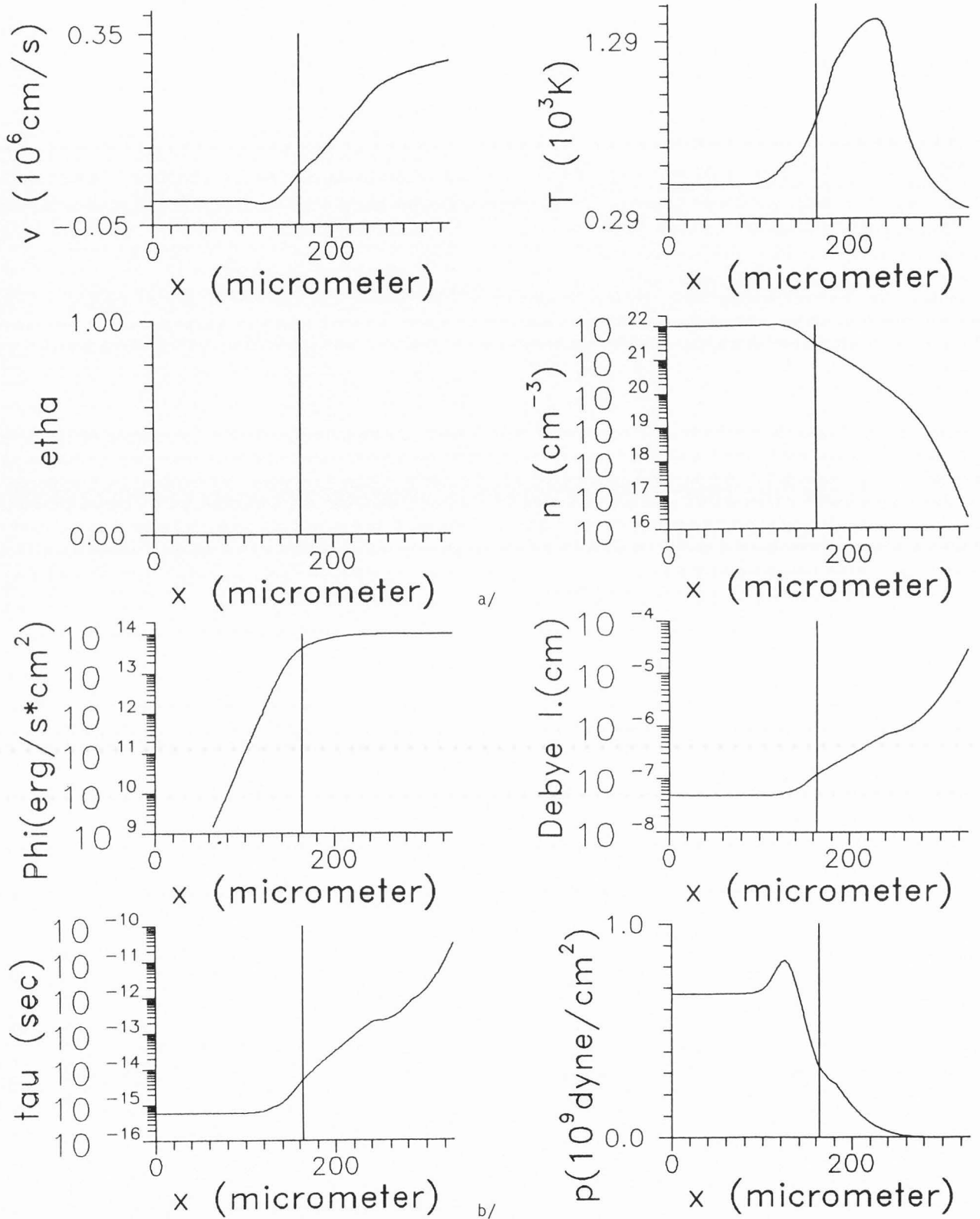
A. Vertes, P. Juhasz, M. De Wolf and R. Gijbels

Figure 7. Ruby laser heating of a target without plasma ignition after $50 nsec$, at low power densities ($10^7 W/cm^2$). a/ velocity, temperature, ionization degree and lg(density) profiles across the interface, b/ light intensity, Debye length, collision time and pressure profiles. See detailed conditions of the calculation in the text.
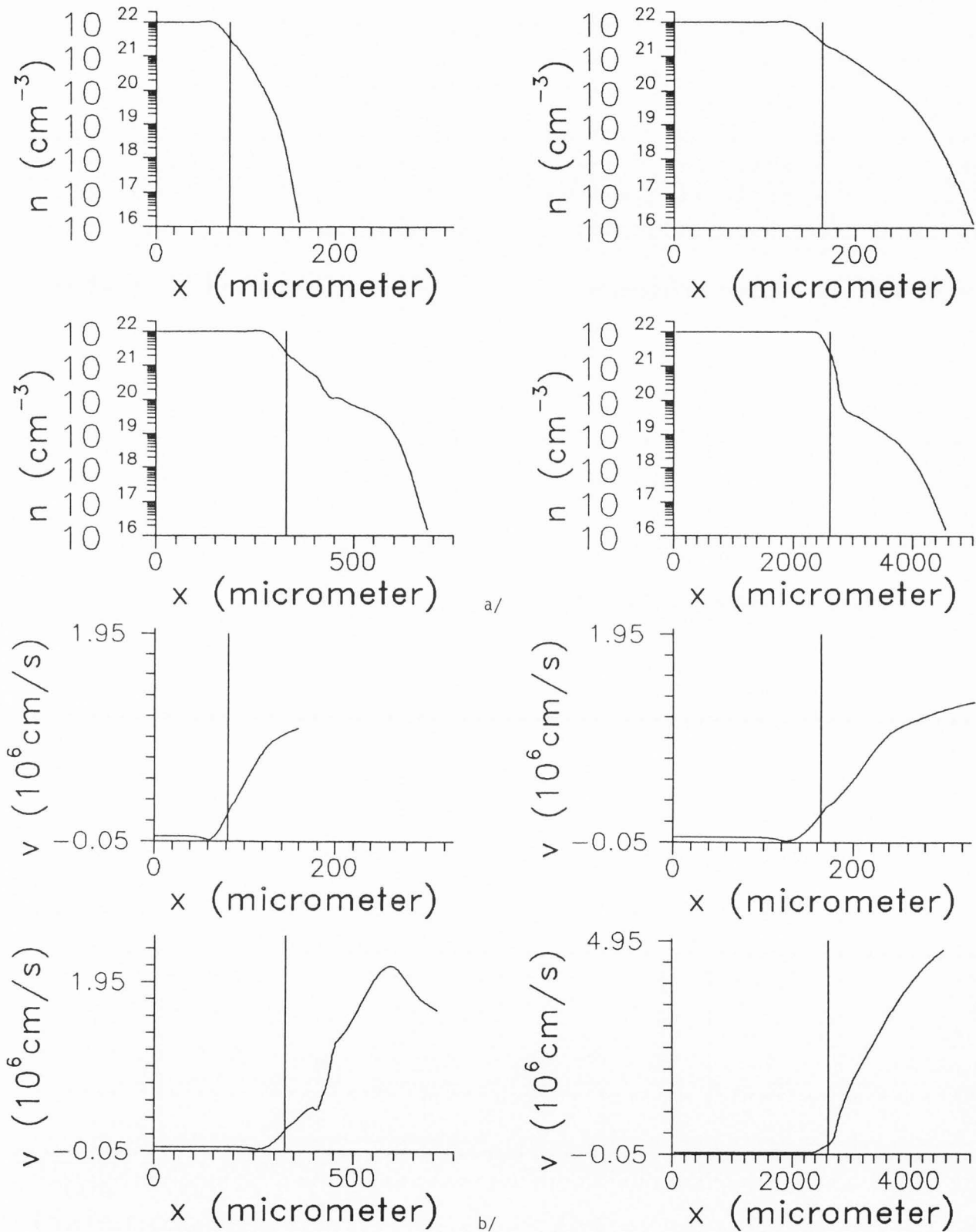
Figure 8. Time development of changes at high power density ($10^9 W/cm^2$) irradiation of the same target as in Fig.7 with resonant plasma absorption. a/ lg(density) and b/ velocity profiles at $7nsec$, $12nsec$, $21nsec$ and $50nsec$, respectively. Notice the difference in the units of the horizontal axis at different times.

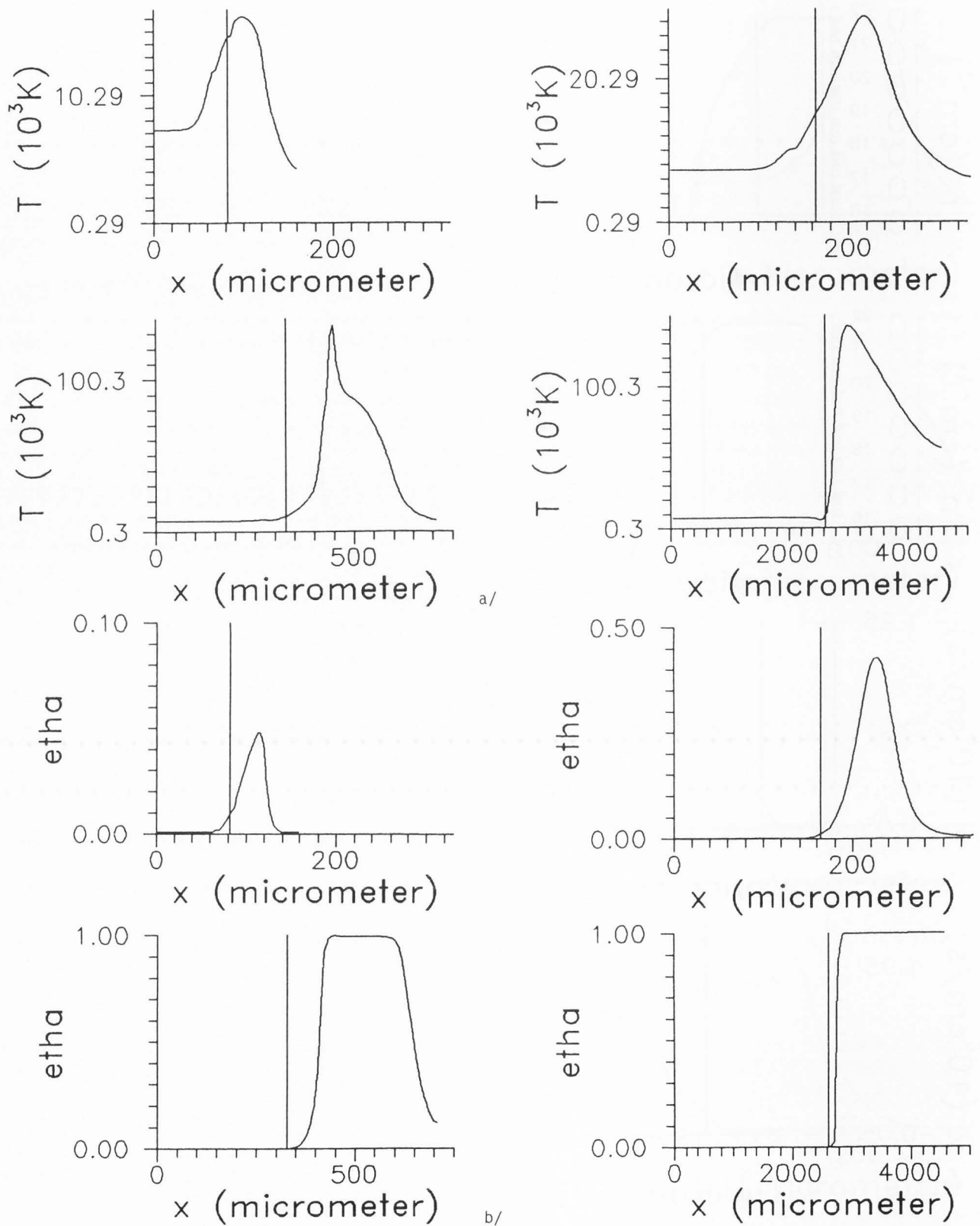A. Vertes, P. Juhasz, M. De Wolf and R. Gijbels

Figure 9. a/ temperature and b/ ionization degree profiles in the same calculation as in Fig. 8. Total ionization and resonant absorption is demonstrated on the curves corresponding to 21nsec and 50nsec.
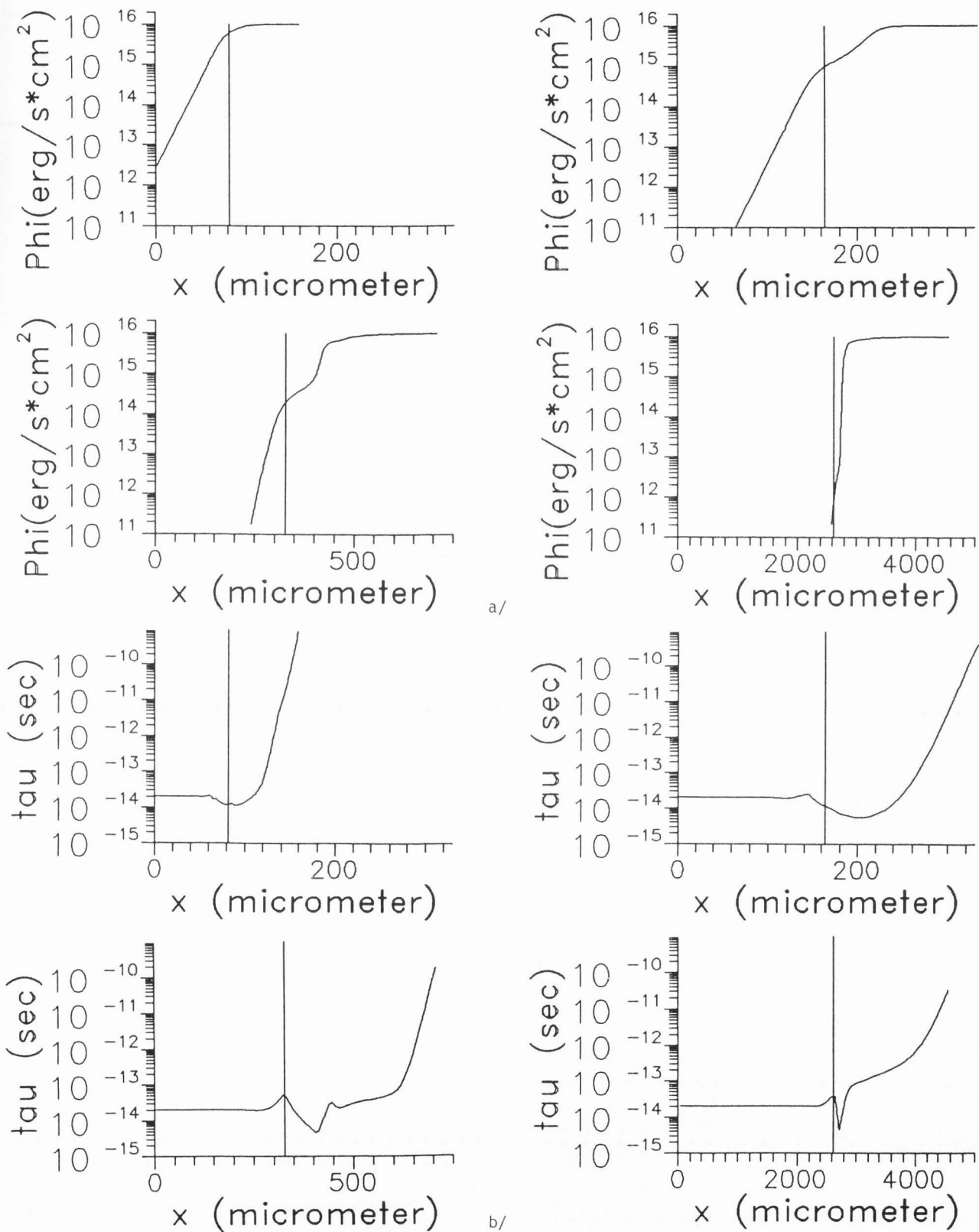
Figure 10. a/ light intensity and b/ collision time profiles in the case described in Fig. 8. Heavy light absorption is identified in the late phase of the interaction. At $50 nsec$ the light even doesn't penetrate the target, since the non-absorbed light is totally reflected causing gradual cooling in the solid phase.
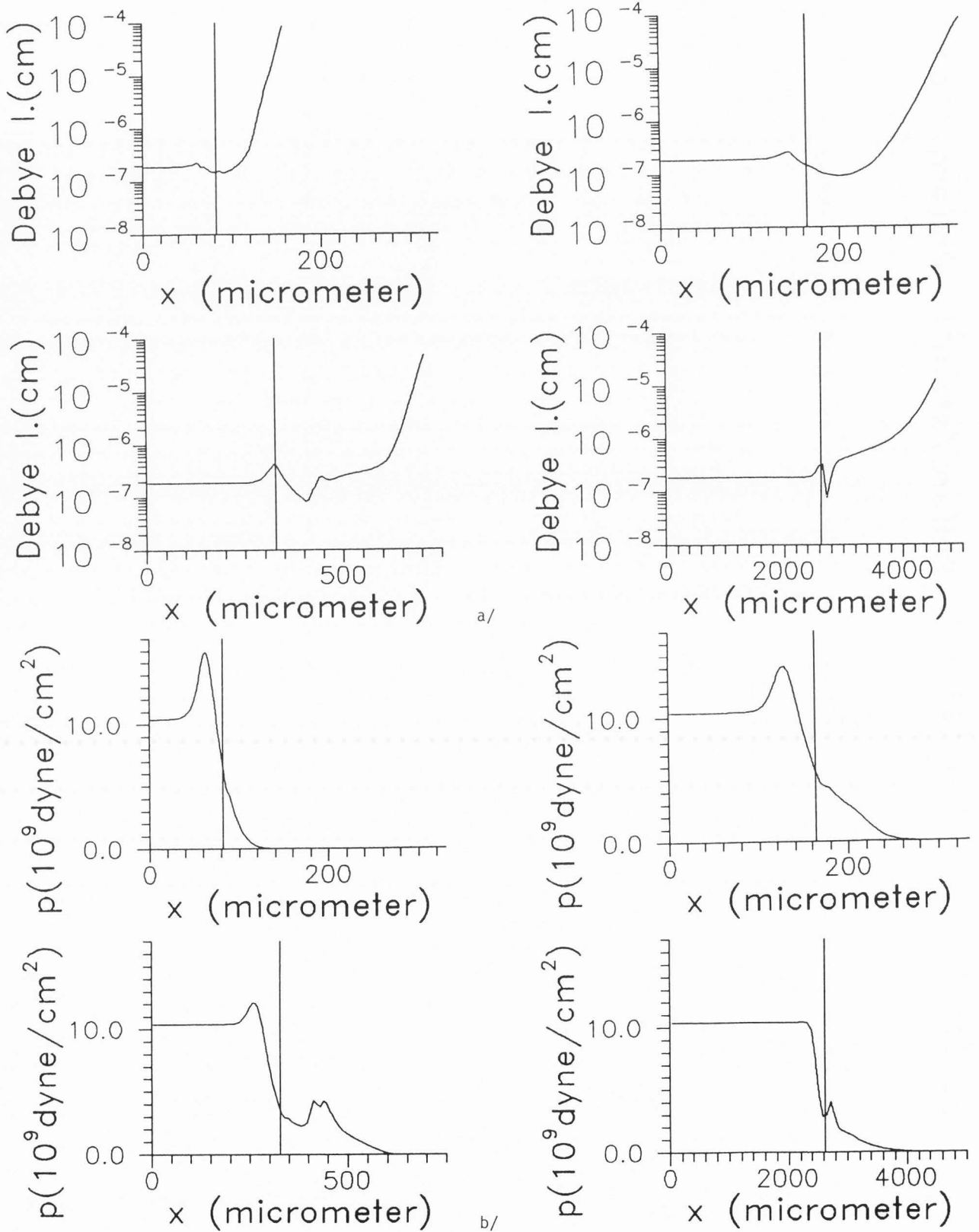
Figure 11. a/ Debye length and b/ pressure profiles in laser target interaction (conditions as in Fig. 8). Compression and shock waves are present in the pressure profiles emphasizing the importance of hydrodynamic effects.

only simple heating was present giving rise to some $1400K(0.12eV)$ in the gas phase. The velocity of the expanding gas reached $2*10^5 cm/sec$, i.e., $0.5eV$ kinetic energy for $M/Z = 24a.m.u.$ particles.

Inspecting Figs. 8, 9, 10 and 11 unfolds the time development of the resonant plasma absorption with positive feedback. The applied higher power density, $\Phi_0 = 10^9 W/cm^2$, already at $7.2nsec$ causes a noticeable increase in the degree of ionization. This increases tenfold in the next five nsec and reaches complete ionization in a layer after $21nsec$. In the remaining $29nsec$ the electron density reaches its critical value leading to resonant absorption in a layer and complete reflection of the non-absorbed light (see Fig. 10/a). This in turn causes some cooling in the target. Peak temperatures reach $1.4*10^5 K(12eV)$ in the gas phase and peak kinetic energy calculated from the velocity $(4*10^6 cm/sec)$ increases to $200eV$. These values are in reasonable agreement with experimental observations (see Figs. 4 and 5).

It is, however, more important to learn from the calculations that the power density, pulse duration, τ_{pulse}, and classical absorption play complementary roles. The total amount of deposited energy roughly estimated in the adiabatic case by $\Phi_0 \tau_{pulse} \alpha_0$ will determine whether plasma ignition takes place or not. This idea is supported by the experiments of Karas et al. (1983, 1985, 1987). They showed that classical absorption and plasma formation thresholds are directly related in the case of several organic compounds. Even enhanced ionization of a non-absorbing compound in an absorbing matrix was observed. This observation gave rise to the technique of "matrix assisted laser desorption". Heinen (1981) has also noticed that the energy coupled from the laser to the target and not the laser power density alone determine the characteristics of laser desorption spectra of organic compounds and inorganic salts.

It is worth noting the difference between the energy calculated from the temperature and from the velocity since the difference shows the fate of the deposited energy. The large excess of kinetic over thermal energy in the case of intense irradiation indicates strong coherent motion in the target, i.e., the presence of shock waves. Accordingly in Fig. 11/b the pressure profiles at $21nsec$ and at $50nsec$ show significant peaks in the gas phase.

Direct comparison of the experimental kinetic energy spectra of particles with the results of the present calculation is possible. Starting from the velocity profiles we can create kinetic energy profiles. Eliminating the space variable from the ion number density and kinetic energy profiles we arrived at the calculated spectra shown in Figs. 12/b and 13/b.

In Fig. 12/a (ii) kinetic energy spectrum of Na^+ ions generated in low power density laser desorption experiments is displayed together with the results of our calculations, Fig 12/b. Although actual shape of the curves is not comparable because of the difference in
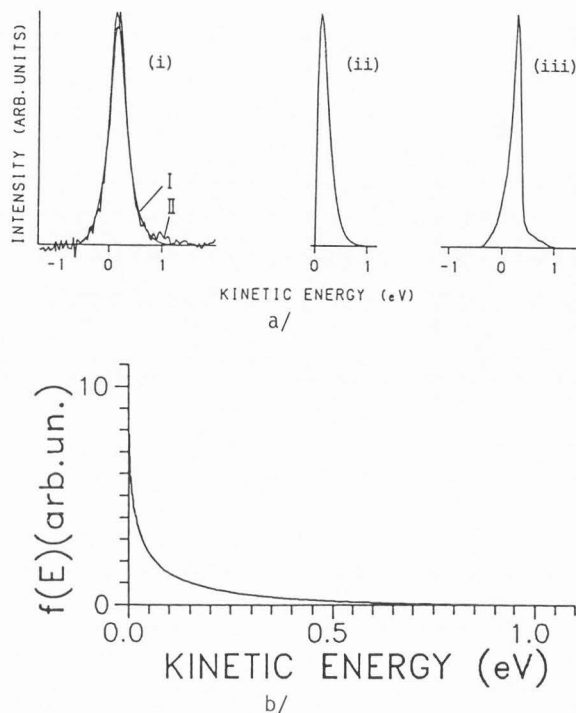

Figure 12. Measured, a/, and calculated, b/, ion kinetic energy distributions in the case of low power density spectra. Measured curves are taken from Van Der Peyl et al., 1984, who investigated Na^+ ion emission from an organic target at $10^7 W/cm^2 CO_2$ laser power density. (i) measured distribution, (ii) deconvoluted energy distribution and (iii) apparatus transmission function. Conditions for the calculated curve are the same as for Fig. 7.

vertical units, agreement in the horizontal extension of the spectra is surprising. Since we have no information about the classical absorption coefficient of the measured samples the degree of agreement is more of a lucky coincidence.

In Fig. 13/a (i) the energy spectrum of Ta^+ ions produced by high power density laser irradiation is shown. Although the absorption coefficient of the sample is not known again, the extension of some $200eV$ of the calculated spectrum is comparable to the $600eV$ range of the measured spectrum. The lower range of calculated energy values can be accounted for to a large extent by the 25 times lower power densities applied in the calculations.

Energy deficient ions

There is another set of observations related to the negative energy part of the kinetic energy spectrum. Their appearance is strongly correlated to the presence or absence of external electric fields as is demonstrated in Fig. 4. (In microprobe situations this external field is always present in the form of accelerating voltage. En-

opment of the ionization degree profiles. One can notice that the degree of ionization and consequently the number density of ions reaches its maximum in the accelerating region before the target plane. This forward shift is a function of time and the values for our conditions are: $40\mu m$ at $7nsec$, $70\mu m$ at $12nsec$, $100\mu m$ at $21nsec$ and $300\mu m$ at $50nsec$. Considering $6kV/cm$ external field strength which is customary in a laser ionization source these values correspond to $24eV, 42eV, 60eV$ and $180eV$ kinetic energy deficit, respectively. This last value is surprisingly close to the extension of the negative tail in Fig. 5.

According to the energy deposition concept we can use the intermediate time profiles as they would be final profiles of a different power density pulse. Since the deposited energy can be roughly estimated by $\Phi_0\tau_{pulse}\alpha_0$, one would expect similarity between the profiles of $\Phi_0 = 10^9W/cm^2$ at $7nsec$ and $\Phi_0 = 1.4*10^8W/cm^2$ at $50nsec$. This approximation is valid only in the limit where absorption is much faster than expansion and the light pulse as well as the absorption coefficient profile are approximated by a step function. The reliability of this approach is also influenced by the relaxation time of internal energy redistribution. The faster these processes are the more realistic profiles we get.

Accepting this argument it can be demonstrated that not only the accelerating field strength determines the extension of the negative energy tail (as it is shown in Fig. 4) but it is correlated with the laser power density too (see in Fig. 5). On the basis of the previous discussion under the given conditions the $180eV$ negative energy tail at $\Phi_0 = 10^9W/cm^2$ would shrink to $24eV$ at $\Phi_0 = 1.4*10^8W/cm^2$. The same decrease could be produced by lowering the accelerating field strength to $0.8kV/cm$ from its original $6kV/cm$ value or more interestingly changing the α_0 absorption coefficient appropriately.

Local thermal equilibrium: estimation of validity

Let us consider in more detail what is necessary to reach the LTE . In general one would expect equilibrium if the residence time of the particles in the interaction zone exceeds the relaxation time of all the nonequilibrium processes. Since under the plasma formation regime the energy of the radiation is coupled to the target by the electrons the first condition is that the electron and ion temperature should be the same:

$$T_e = T_i. \qquad (26)$$

This is satisfied only for times larger than the $t_{\Delta T_{ei}}$ temperature relaxation time:

$$t_{\Delta T_{ei}} = \frac{1}{2}\frac{m_i}{m_e}\frac{n_i}{n_i + n_e}\tau_{ei}. \qquad (27)$$

The right hand side can be simplified to $459M_i\tau_{ei}$ if $n_e = n_i$ is maintained. M_i denotes the ionic mass
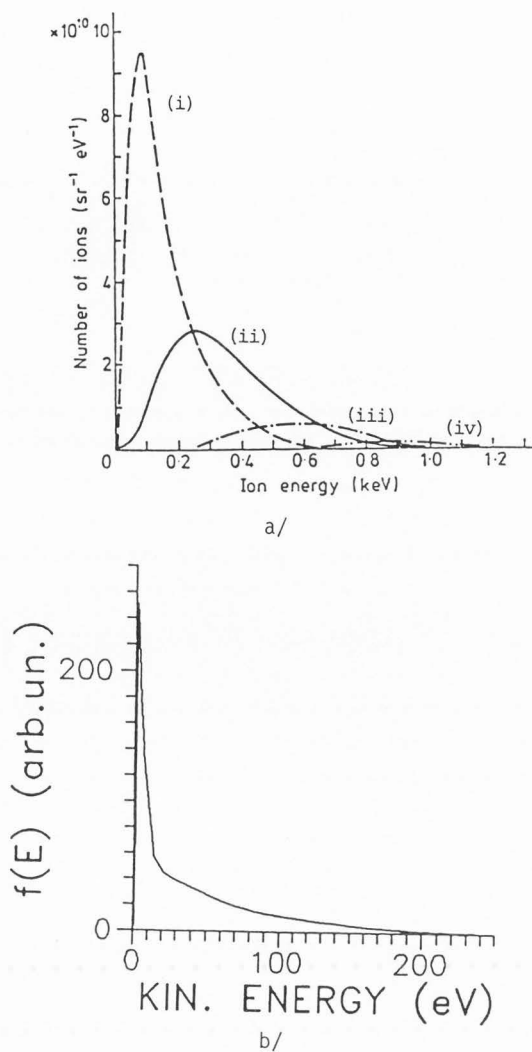

Figure 13. Experimental (Dinger et al., 1980), a/, and calculated, b/, kinetic energy distributions for high laser power density irradiation. The experimental conditions were: $Nd - YAG$ laser at $2.5 * 10^{10}W/cm^2$ hitting a tantalum target. The curves (i), (ii), (iii) and (iv) correspond to Ta^+, Ta^{2+}, Ta^{3+} and Ta^{4+}. The calculations had the same parameters as in Fig. 8.

ergy distributions of SIMS ions with negative energy tails were published for instance by Lodding, 1988.) These and other similar evidence (Mauney and Adams, 1984, Michiels et al., 1984) prompt the idea that ion formation may take place before the target plane as well, allowing reduced acceleration of these ions.

The two most probable ways of producing ions in the accelerating field are either laser ionization of the expanding neutrals or their reaction with other particles such as ionic species or electrons (Rosmarinowsky et al. 1985). Our model provides the possibility to follow the first mechanism. In Fig. 9/b we trace the time devel-

in a.m.u. Visualization of typical collision time profiles at the vacuum - target interface can be seen in Figs. 7/b and 10/b. To obtain $t_{\Delta T_{ei}}$ these curves should be shifted 4 orders of magnitude upward in the case of $M/Z = 24$ a.m.u. ions. It is demonstrated that the electron - ion collision time in the dense part of the plasma is much smaller than the mean residence time of the particles, τ_{res} which in LIMS situations is typically in the neighborhood of 100 nsec. This means that the equilibrium of the electron and ion temperatures is usually reached, furthermore the one component energy equation can be used. However, it is also worthwhile to notice that the outer surface of the plasma is not always necessarily in equilibrium. In this region even the hydrodynamic equations cannot be used since no collision happens in a single time step at the final phase of the calculation. Fortunately this region has no real importance in the evaluation since a vanishingly small fraction of the material can be found here.

On the basis of Eq. (27) we can understand the capability of ionization by laser of volatile large molecular weight organic compounds. Taking, for example, the laser ionization of $M/Z = 240$ a.m.u. particles the temperature relaxation times will cover the $10^{-10} - 10^{-6} sec$ range. Comparing this to the mentioned upper limit for residence time in the source it is clear that non-negligible amount of the ions will not reach the T_e temperature. This practically means less fragmentation and strongly non-LTE behavior. The present argument may throw light on one of the main attractions of laser ionization of solid targets, namely the possibility of ion production of large volatile organic molecules without fragmentation.

So far we have considered only the energy exchange between electrons and ions. In reality a vast number of other elementary processes are generated in the plasma. These all can be characterized by rate equations and corresponding time constants. Classes of these processes are the following.

a/ Radiative excitation and decay:

$$A(q) + h\nu \rightleftharpoons A(q+r). \tag{28}$$
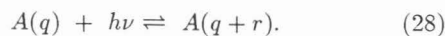
Radiative excitation is very unlikely since a nonvanishing transition probability exists only under resonance conditions. It is achievable with finely tuned dye lasers but the corresponding resonance ionization spectroscopy (RIS) will not be discussed here.
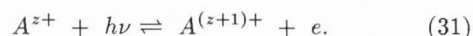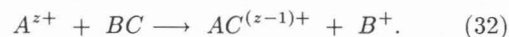
b/ Collisional excitation and decay:

$$A(q) + e \rightleftharpoons A(q+r) + e. \tag{29}$$
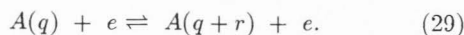
c/ Collisional ionization and recombination:

$$A^{z+} + e \rightleftharpoons A^{(z+1)+} + e + e. \tag{30}$$
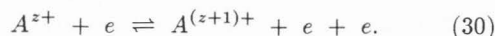
d/ Radiative ionization and recombination:

$$A^{z+} + h\nu \rightleftharpoons A^{(z+1)+} + e. \tag{31}$$

e/ Ion - molecule reactions:

$$A^{z+} + BC \longrightarrow AC^{(z-1)+} + B^+. \tag{32}$$

f/ Fragmentation:

$$AB + e \longrightarrow A^+ + B + 2e. \tag{33}$$
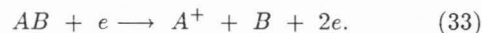
We may describe the time constant of only the collisional (and not the radiative) processes roughly by the absolute rate theory:

$$\tau_{rate} = \tau_c \, exp\left(\frac{E^*}{kT}\right). \tag{34}$$

where τ_c is the collision time of the reacting particles and E^* is the so called activation energy of the process. The collision time is generally determined by the kinetic theory but corrections are necessary when charged particles are taking part since Coulomb or induced dipole attraction makes the encounters more probable.

The time constant of the radiative decay and radiative ionization processes can be determined empirically (Yasuda and Sekiguchi, 1979).

Real equilibrium concentration of the ionic species is reached only when all reaction time constants are considerably smaller than the τ_{res} residence time. This puts an upper limit on the activation energy:

$$E^* \ll kT \, ln\left(\frac{\tau_{res}}{\tau_c}\right). \tag{35}$$

In the case of high power density irradiation this expression can be evaluated on the basis of Figs. 9/a and 10/b. In the outer region of the expanding plasma the condition for E^* is: $E^* \ll 47.6eV$. Similar estimation on the basis of Fig. 7 for the low power density case gives: $E^* \ll 0.32eV$. Since most activation energies for ordinary rate processes lie below $20eV$ they reach equilibrium readily at high irradiances. Surprisingly, however, reaching LTE from the point of view of collisional rate processes at low laser power densities is not that obvious anymore.

The situation is different in the case of radiative processes, where higher power density means higher number density of photons. Consequently reaching LTE with the radiation field takes more time than in the low power density case.

Hydrodynamic effects

Further consequences of our model can be observed in Figs. 11/b and 8/a. As expected two waves emerge

from the decaying interface, a compression wave moving to the left and a shock wave moving to the right.

In the early phase of laser heating the compression wave is dominant. At $7 nsec$ as much as 50% overpressure and 10% compression in density was observed. This overdense region is not identifiable in Fig. 8/a because the density is on logarithmic scale. Linear plots of density against position clearly show a density peak in the solid phase. At later stages this wave penetrates into the solid and gradually decays. The finite negative velocity of this wave appears in Fig. 8/b. Experimental evidence for this effect is the perforation of finite thickness targets and traces of splashed material around the craters in block samples.

Other hydrodynamic phenomenon can be recognized in Fig. 11/b. The pressure profiles at $21 nsec$ and at $50 nsec$ exhibit pronounced peaks in the expansion region. This peak travels in the low pressure direction and becomes apparent only in the late phase of laser heating. Since the pressure profile varies together with the internal energy density profile this maximum also means that part of the internal energy of the plasma travels together with this wave. Comparing the ionization degree, light intensity and pressure profiles show that it is in these waves that strong ionization and heavy absorption takes place.

Examining the third component of the generalized density vector, Eq. (17), one can estimate the importance of hydrodynamic energy compared to internal energy. It is the relation of e toward $v^2/2$ that decides which effects are more important. Apparently we have already seen above in the case of these model calculations that both energy parts are on the same scale. However it is also demonstrated that the importance of hydrodynamic effects increases with laser power density in accordance with the observations of Chiarelli and Gross (1987), for example. In the extreme high power density limit (above $10^{13} W/cm^2$) even ablative acceleration of thin foils was found by Raven et al. (1981). That could explain the disintegration of the removed foil part in terms of Rayleigh - Taylor type hydrodynamic instabilities.

Atomization vs. ionization

There is another mechanism of energy deposition which in nuclear fusion studies is usually considered negligible compared to the previously described forms. Since the target is normally a solid the heat of melting and evaporation or the heat of sublimation has to be added to the energy balance of the processes (Afanasyev et al. 1966). Nevertheless in the case of molecular solid targets partial or complete fragmentation takes place where the rupture of chemical bonds of the molecules is also a method of energy absorption. Cluster surface energies (Campana et al. 1981) and cluster internal energies (Hoogerbrugge and Kistemaker 1987) are also discussed as possible governing factors of ion abundance distributions.

The conventional target of nuclear fusion experiments is more of an exception from the point of view of atomization since its ratio of first ionization energy and atomization energy is $I_p^H/E_{at}^H \approx 3000$. Taking, for example, the carbon target this value drops to $I_p^C/E_{at}^C \approx 1.5$ only. Typical values for metals and semiconductors are: $I_p^{Na}/E_{at}^{Na} \approx 4.9$, $I_p^{Fe}/E_{at}^{Fe} \approx 2.15$, $I_p^{Si}/E_{at}^{Si} \approx 4.6$ and $I_p^{Ge}/E_{at}^{Ge} \approx 2.7$. It is the richness of laser ionization spectra in cluster ions which shows the importance of the atomization process. Since the removal of clusters takes less energy than complete atomization and the surface energy of clusters also changes with cluster configuration (Campana et al., 1981) no precise prediction can be made about the fate of the above mentioned ratio.

A more general form of internal energy density should include the atomization and fragmentation process as well and could be approximated:

$$ e = \frac{1}{m}\left[\frac{3}{2}(1+\eta)kT + \eta I_p + \xi E_{at} + \frac{m}{m_i}\sum_i \chi_i E_{bond,i}\right], \tag{36} $$

where ξ is the degree of atomization, most simply a step function changing from zero in the solid to one in the gas phase at the boiling point temperature. The last term of Eq. (36) is a rough estimation of the energy invested in fragmentation. It is formulated as a weighted average of binding energies, $E_{bond,i}$, over each broken bond denoted by i. χ_i denotes the weighting factor. Solving the hydrodynamic equations with this form of energy density would give direct information about the depth of atomization behind the target plane, i. e., direct calculation of crater depths would be possible (measured values see, for example, Narayan 1979). The melting process, at least in the case of elements, is really negligible compared to evaporation, consuming normally at least one order of magnitude less energy than the atomization energies.

Strong lateral gradients

Although we accounted only for events going on perpendicular to the target plane there are clear indications that in the case of strong lateral inhomogeneity, in plane processes may play an equally important role (Day et al., 1981). It is also enough to mention the different spectra we get in the transmission mode of operation if part of the supporting SEM grid was also hit by the laser beam. No need to say, targets with microstructure (i.e., lateral inhomogeneity) are the most important subjects of microprobe investigations. It is also believed that some of the problems with the reproducibility of LIMS spectra are related to undiscovered lateral variations of concentration, absorption coefficient, etc.

As was shown earlier, the main way of laser target coupling is through normal absorption at the wavelength of the laser light. So, for example, in the case of visible light inspection and UV light ionization it can happen that one doesn't notice the inhomogeneity with the naked eye yet still get different spectra from the different

points of the sample.

Let us consider a target having very low and very high transmission on the two halves of the focal spot. It is obvious that illuminating the transparent part only, would give no ionization at all. So the situation can be described as *induced plasma ignition* and treated like lateral mixing of two clouds with extreme temperature difference.

After some ionization of the transparent part has been induced, it may also become opaque and absorb heavily. Assuming adiabatic absorption of the light, one would expect a temperature difference, $T_2 - T_1$, between the two parts at time t determined by:

$$\frac{3}{2}n\left[(1 + \eta_2)kT_2 - (1 + \eta_1)kT_1\right] + \eta_2 I_{p,2} - \eta_1 I_{p,1} =$$

$$= (\alpha_{0,2} - \alpha_{0,1})\Phi_0 t \ . \tag{37}$$

Solving this equation together with the two Saha type equations can account for the situation before expansion and mixing.

Since gradients laterally can be enormous too, strongly turbulent mixing together with reactions are expected. Description of these processes exceed the limits of the present paper but it can well be understood that LIMS spectra are extremely sensitive to lateral variations in absorption coefficient. Similar effects are expected in the case of strong variations in sample thickness, i.e., for example in the case of particles comparable in size to the focal spot.

Summary

Similarities between secondary ionization and laser ionization processes inspired us to make a comparative but brief review of the theories on the two fields. The success of the *energy deposition and redistribution concept* in the description of SIMS promised more precise understanding of the LIMS processes too. The enormous differences in the number of elementary events, however, required different methods of description for SIMS and LIMS. While the ion-beam target interaction was most effectively explained by kinetic and molecular models, a more suitable method for the investigation of laser ionization seemed to be its description by *hydrodynamic formalism*.

We set up a simple one component - one dimensional *(1C-1D)* model in order to demonstrate its capabilities to reflect important experimental findings in LIMS. Estimation of the extent of non-linear light absorption showed no significance under customary circumstances.

Extreme initial conditions due to the solid - vacuum interface and severe excitation due to the immense laser pulse hampered the finite difference solution of the partial differential equations describing the conservation of mass, momentum and energy. Application of Godunov's first scheme together with adaptive grids as a reference frame provided an appropriate solution to the problem.

Model calculations on ruby laser semi-infinite target interaction were carried out and showed the following interesting features. In accordance with the experiments, clear distinction could be made between *laser desorption*, based mainly on classical absorption at low light power densities and *laser plasma ionization* ignited by resonant plasma absorption at high irradiances.

If no external electric field was present promising kinetic energy distributions of the generated ions were recovered from our calculations. Comparison of the extension of spectra in the two limiting cases with experimental curves showed considerable correlation. The appearance of energy deficient ions in an external electric field was rationalized in terms of ionization before the target plane resulting in reduced acceleration. Estimation of the effect based on the forward shift of maximal degree of ionization gave feasible results.

Calculation of electron - ion collision time profiles across the interface made it possible to obtain a more detailed picture about the validity of the local thermal equilibrium hypothesis. One of the strongest conditions to reach LTE is the equilibration of the electron and ion temperatures. While for low mass ions LTE is usually achieved in this respect, the relaxation time for the energy exchange process turned out to be a linear function of the ionic mass. This explains the possibility of laser ionization of large volatile molecules without degradation. Other elementary collisional processes have to reach equilibrium too. In the case of a high activation energy requirement LTE is more easily reached at high power densities.

At increased irradiances two interesting hydrodynamic effects were identified in the calculations: a compression wave travelling from the interface towards the bulk and a shock wave running in the opposite direction. The place of heavy light absorption and strong ionization was correlated with the position of the shock wave. The importance of hydrodynamic effects increased with increasing laser power density.

The role of atomization was discussed in relation with energy redistribution. Competition of atomization and ionization processes for the deposited energy can be expressed in terms of their energy requirements enlightening the basic difference between solid hydrogen and other targets in this respect. Inclusion of the effects of atomization in the hydrodynamic model would certainly be quite interesting.

Finally we addressed the problem of strong lateral gradients which is rather important in microprobe experiments. Inhomogeneity in the absorption coefficient of the target inside the focal spot may lead to enormous temperature differences. If one part of the illuminated surface absorbs enough energy for plasma ignition it can induce ionization and strong absorption on other parts too, due to lateral expansion and mixing. These poorly controllable processes may provide the key to the under-

standing of ill reproduced LIMS spectra in some cases.

Acknowledgement

References

Afanasyev YU, Krokhin ON, Sklizkov GV. (1966). Evaporation and heating of a substance due to laser radiation. IEEE J. Quant. Electr. $\underline{3}$, 9:483-486.

Ahmad S, Farmery BW, Thompson MW. (1980). The effect of ion mass and target temperature on the kinetic energy distribution of sputtered atoms. Nucl. Instr. Meth. $\underline{170}$, 327-330.

Andersen CA. (1975). A critical discussion of the local thermal equilibrium model for the quantitative correction of sputtered ion intensities. Nat. Bur. Stand. Spec. Publ. $\underline{427}$, 79-119.

Benninghoven A, Rüdenauer FG, Werner HW. (1987). Secondary ion mass spectrometry. Wiley. New York. 7-329.

Biersack JP, Haggmark LG. (1980). A Monte Carlo computer program for the transport of energetic ions in amorphous targets. Nucl. Instr. Meth. $\underline{174}$, 257-269.

Braginskii SI. (1965). Transport processes in a plasma. In: Reviews of plasma physics; H.A. Leontovich (ed). Consultant Bureau. New York. Vol. 1. 205-311.

Campana JE, Barlak TM, Colton RJ, DeCorpo JJ, Wyatt JR, Dunlap BI. (1981). Effect of cluster surface energies on secondary-ion-intensity distributions from ionic crystals. Phys. Rev. Lett. $\underline{47}$, 15:1046-1049.

Caruso A, Gratton R. (1968). Some properties of the plasmas produced by irradiating light solids by laser pulses. Plasma Physics. $\underline{10}$, 867-877.

Castaing R, Slodzian G. (1981). Analytical microscopy by secondary ion imaging techniques. J. Phys. E: Sci. Instr. $\underline{14}$, 1119-1127.

Chiarelli MP, Gross ML. (1987). Mechanism of cationization of sucrose by sodium in laser desorption : a study by Fourier transform mass spectrometry. Int. J. Mass Spectrom. Ion Proc. $\underline{78}$, 37-52.

Chowdhury SS, Clement RM, Miles HT. (1980). Ion energy analyser for laser-produced plasma. J. Phys. E: Sci. Instr. $\underline{13}$, 1099-1105.

Conzemius RJ, Capellen JM. (1980). A review of the applications to solids of the laser ion source in mass spectrometry. Int. J. Mass Spectr. Ion Phys. $\underline{34}$, 197-271.

Dawson J, Kaw P, Green B. (1969). Optical absorption and expansion of laser-produced plasmas. Phys. Fluids. $\underline{12}$, 4:875-882.

Day RJ, Forbes AL, Hercules DM. (1981). Laser desorption mass spectrometry of some organic acids. Spectrosc. Lett. $\underline{14}$, 10:703-727.

Demtröder W, Jantz W. (1970). Investigation of laser-produced plasmas from metal-surfaces. Plasma Phys. $\underline{12}$, 691-703.

de Vries AE. (1987). Sputtering of molecules and clusters. Nucl. Instr. Meth. Phys. Res. B $\underline{27}$, 173-180.

Dinger R, Rohr K, Weber H. (1980). Ion distribution in laser produced plasma on tantalum surfaces at low irradiances. J. Phys. D: Appl. Phys. $\underline{13}$, 2301-2307.

Drawin HW. (1971). Thermodynamic properties of the equilibrium and nonequilibrium states of plasmas. In: Reactions under plasma conditions. Vol. I.; M. Venugopalan (ed), Wiley. New York. 53-238.

Eloy JF. (1985). Geological applications of ionization LTE model in laser probe mass spectrometry. Scanning Electron Microsc. 1985; II:563-576.

Eloy JF. (1986). Quantitative microanalysis by time-of-flight laser probe mass spectrometry. Scanning Electron Microsc. 1986; IV:1243-1253.

Furstenau N. (1981). Investigation of laser induced damage, evaporation and ionization with homogeneous inorganic target foils. Fresenius Z. Anal. Chem. $\underline{308}$, 201-205.

Gerhard W. (1975). A model calculation of the neutral molecule emission by sputtering processes. Z. Physik B $\underline{22}$, 31-39.

Glasstone S, Laidler KJ, Eyring H. (1941) The theory of rate processes. McGraw Hill. New York. 124-208.

Godunov SK. (1959). A finite difference method for the numerical computation and discontinuous solutions of the equations of fluid dynamics. Mat. Sborn. $\underline{47}$, 271-281.

Goto T, Kishi K, Okuda T. (1982). Energy analysis of multiple charged ion produced by irradiating laser light on solid targets. Karu Jugo Kenryu. $\underline{47}$, 592-599.

Haas U, Wieser P, Wurster R. (1981). A quantitive interpretation of LAMMA spectra based on a local thermodynamic equilibrium (LTE) model. Fresenius' Z. Anal. Chem. 308, 270-273.

Hahn MY, Honea EC, Paguia AJ, Schriver KE, Camarena AM, Whetten RL. (1986). Magic numbers in C_N^+ and C_N^- abundance distributions. Chem. Phys. Lett. 130, 12-16.

Hautala M. (1984). Nuclear stopping in polycrystalline materials: range distributions and Doppler-shift attenuation analysis. Phys. Rev. B 30, 9:5010-5018.

Heinen HJ. (1981). On ion formation in laser desorption mass spectrometry with LAMMA. Int. J. Mass Spectr. Ion Phys. 38, 309-322.

Hillenkamp F. (1983). Laser induced ion formation from organic solids. In: Ion formation from organic solids; A. Benninghoven (ed). Springer Ser. Chem. Phys. 25, 190-205.

Hillenkamp F. (1985). Laser desorption mass spectrometry, a review. In: Secondary ion mass spectrometry, SIMS V; A. Benninghoven (eds). Springer Ser. Chem. Phys. 44, 471-475.

Holt M. (1977). Numerical methods in fluid dynamics. Springer Verlag. Berlin. 33-38.

Hoogerbrugge R, Kistemaker PG. (1987). Analytical expressions for the internal and kinetic energy distributions of sputtered clusters and molecules. Nucl. Instr. Meth. Phys. Res. B 21, 37-45.

Hora H. (1979). Nonlinear plasma dynamics at laser irradiation. Springer Verlag. Berlin. 19-75.

Husinsky W, Bruckmüller R, Blum P. (1980). Velocity measurements of sputtered particles using the laser-Doppler method. Nucl. Instr. Meth. 170, 287-293.

Johnson RE. (1987). Mechanisms for the desorption of large organic molecules. Int. J. Mass Spectr. Ion Proc. 78, 357-392.

Karas M, Bachmann D, Hillenkamp F. (1983). Investigations into the ion formation mechanisms in LAMMA analysis : wavelength dependence of ion formation from aromatic and aliphatic amino acids. LAMMA Workshop 1983, Forschunginstitute Borstel (F.R.G.). 9-10.

Karas M, Bachmann D, Hillenkamp F. (1985). Influence of the wavelength in high irradiance ultraviolet laser desorption mass spectrometry of organic molecules. Anal. Chem. 57, 2935-2939.

Karas M, Bachmann D, Bahr U, Hillenkamp F. (1987). Matrix assisted ultraviolet laser desorption of non-volatile compounds. Int. J. Mass Spectr. Ion Proc. 78, 53-68.

Kidwell DA, Ross MM, Colton RJ. (1987). A mechanism of ion production in secondary ion mass spectrometry. Int. J. Mass Spectrom. Ion Proc. 78, 315-328.

Krueger FR. (1983). Thermodynamics of ion formation by fast dissipation of energy at solid surfaces. Z. Naturforsch. 38 a, 385-394.

LaiHing K, Wheeler RG, Wilson WL, Duncan MA. (1987). Photoionization dynamics and abundance patterns in laser vaporized tin and lead clusters. J. Chem. Phys. 87, 6:3401-3409.

Littmark U, Sigmund P. (1975). Momentum deposition by heavy ion bombardment and an application to sputtering. J. Phys. D: Appl. Phys. 8, 241-245.

Lodding A. (1988). Secondary ion mass spectrometry. In: Inorganic mass spectrometry; F. Adams, R. Gijbels, R. Van Grieken (eds), Wiley, New York, 140-145.

Mauney T, Adams F. (1984). Ion kinetic energy measurements on laser-induced plasmas in laser microprobe mass analysis (LAMMA). Part I. Methodology. Int. J. Mass Spectr. Ion Proc. 59, 103-119.

Michiels E, Mauney T, Adams F, Gijbels R. (1984). Ion kinetic energy measurements on laser-induced plasmas in laser microprobe mass analysis (LAMMA). Part 2. Titanium dioxide. Int. J. Mass Spectr. Ion Proc. 61, 231-246.

Mulser P. (1970). Hydrogen plasma production by giant pulse lasers. Z. Naturforsch. 25 a, 282-295.

Mulser P. (1971). Electrostatic fields and ion separation in expanding laser produced plasmas. Plasma Physics. 13, 1007-1012.

Narayan J. (1979). Depth of melting produced by pulsed laser irradiation. Appl. Phys. Lett. 34, 5:312-315.

Newbury DE. (1980). Methods for quantitative analysis in secondary ion mass spectrometry. Scanning 3, 110-118.

Odelius H, Lodding ARE, Werme LO, Clark DE. (1985). Secondary ion mass spectrometry of glasses : aspects of quantification. Scanning Electron Microsc. 1985; III:927-934.

Ramendik GI, Manzon BM, Tiurin DA, Benyaev NE, Komleva AA. (1987). Perspectives in the development of the theory of spark-source and laser-plasma source mass spectrometry. Talanta 34, 1:61-67.

Ramendik G., Verlinden J, Gijbels R. (1988). Spark source mass spectrometry. In: Inorganic mass spectrometry; F. Adams, R. Gijbels, R. Van Grieken (eds). Chem. Anal. Ser. 95, Wiley. New York. 17-84.

Ramendik GI, Derzhiev VI, Surkov YA, Ivanova VF, Grechishnikov AV. (1981). Real energy spread of ions produced in vacuum spark-discharge plasma. Int. J. Mass Spectr. Ion Phys. 37, 331-339.

Raven A, Azechi H, Yamanaka T, Yamanaka C. (1981).

Stability of ablatively accelerated thin foils. Phys. Rev. Letters. 47, 15:1049-1053.

Robinson MT, Torrens IM. (1974). Computer simulation of atomic displacement cascades in solids in the binary collision approximation. Phys. Rev. B 9, 12:5008-5024.

Rosmarinowsky J, Karas M, Hillenkamp F. (1985). Metastable decay of laser-desorbed ions from aromatic organic compounds. Int. J. Mass Spectr. Ion Proc. 67, 109-119.

Sack C, Schamel H. (1987). Plasma expansion into vacuum - A hydrodynamic approach. Phys. Reports 156, 311-395.

Sanders JB. (1980). Time evolution of collision induced hot spikes. Radiat. Eff. 51, 43-48.

Schäfer B, Hess P. (1985). Time-of-flight diagnostics of wavelength-dependent CO_2 laser-induced desorption from condensed layers. Appl. Phys. B 37, 197-204.

Seitz F, Koehler JS. (1956). Displacement of atoms during irradiation. In: Solid state physics. Vol. 2.; F. Seitz, D. Turnbull (eds). Academic Press. New York. 305-448.

Siegel MW, Vasile MJ. (1981). New wide angle, high transmission energy analyzer for secondary ion mass spectrometry. Rev. Sci. Instr. 52, 11:1603-1615.

Sigmund P. (1969). Theory of sputtering. I.Sputtering yield of amorphous and polycrystalline targets. Phys. Rev. 184, 2:383 -416.

Sigmund P. (1984). Fundamentals of sputtering. In: Secondary ion mass spectrometry, SIMS IV; A. Benninghoven, J Okano, R. Shimizu and H. W. Werner (eds). Springer Ser. Chem. Phys. 36, 2-7.

Spitzer L. (1962) Physics of fully ionized gases. John Wiley & Sons. New York. 120-154.

Sunner JA, Kulatunga R, Kebarle P. (1986). Secondary ion currents in fast atom bombardment of preionized liquids. Anal. Chem. 58, 2009-2014.

Sunner J, Morales A, Kebarle P. (1988). Kinetic modeling of fast atom bombardment spectra of glycerol - diethanolamine mixtures. Anal. Chem. 60, 98-104.

Swenters K, Verlinden J, Bernard P, Gijbels R. (1986). Electrode surface modification and material transport into a high voltage vacuum spark discharge. Int. J. Mass Spectr. Ion Proc. 71, 85-102.

Swenters K, Verlinden J, Gijbels R. (1987). Applications of spark-source mass spectrometry for localized microanalysis, film analysis and depth analysis. Anal. Chim. Acta. 195, 173-179.

Tabet JC, Cotter RJ. (1983). Time-resolved laser desorption mass spectrometry. II. Measurement of the energy spread of laser desorbed ions. Int. J. Mass Spectr. Ion Proc. 54, 151-158.

Tallents GJ. (1980). An experimental study of recom-

bination in a laser-produced plasma. Plasma Phys. 22, 709-718.

Tallents GJ. (1981). On the fitting of displaced Maxwellians to laser-produced plasma ion velocity distributions. Opt. Commun. 37, 2:108-112.

Thompson DA. (1981). High density cascade effects. Radiat. Eff. 56, 105-150.

Thompson DA, Johar SS. (1980). Sputtering of silver by heavy atomic and molecular ion bombardment. Nucl. Instr. Meth. 170, 281-285.

Trevor DJ, Cox DM, Reichmann KC, Brickman RO, Kaldor A. (1987). Ionizing laser intensity dependence of the silicon cluster photoionization mass spectrum. J. Phys. Chem. 91, 10:2598-2601.

Tsong TT. (1986). Time-of-flight ion energy and ion reaction time spectrometry, spectral line shape and mechanisms of ion formation. Int. J. Mass Spectr. Ion Proc. 70, 1-21.

Van der Peyl GJQ, Van der Zande WJ, Bederski K, Boerboom AJH. (1983). Kinetic energy distribution measurement of laser produced ions. Int. J. Mass Spectrometry Ion Phys. 47, 7-10.

Van der Peyl GJQ, Van der Zande WJ, Kistemaker PG. (1984). Kinetic energy distributions of ions produced in organic laser desorption. Int. J. Mass Spectr. Ion Proc. 62, 51-71.

Van Puymbroeck J, Gijbels R, Viczian M, Cornides I. (1984). Time-resolved measurements in spark source mass spectrometry. II. Detection of the ion current by a fast transient recorder. Int. J. Mass Spectr. Ion Proc. 56, 269- 280.

Vatsya SR. (1987) A representation and approximation of the solutions of hyperbolic differential equations. J. Comp. Phys. 73, 289-305.

Verlinden JAA, Swenters KME, Gijbels RHH. (1985). Modification in the surface composition of sparked electrodes and its relation to relative sensitivity factors in spark source mass spectrometry. Anal. Chem. 57, 1:131-136.

Vertes A, Juhasz P, Jani P, Czitrovszky A. (1988). Kinetic energy distribution of ions generated by laser ionization sources. Int. J. Mass Spectr. Ion Proc. 83, 45-70.

von Neumann J, Richtmyer RD. (1950) A method for the numerical calculation of hydrodynamical shocks. J. Appl. Phys. 21, 232-245.

Whitlow HJ, Hautala M, Sundqvist BUR. (1987). Collision cascade parameters for slow particles impinging on biomolecule targets. Int. J. Mass Spectrom. Ion Proc. 78, 329-340.

Wilson RG, Brewer GR. (1973) Ion beams. Wiley. New York. 179-180.

Wittmaack K. (1979) Secondary-ion emission from silicon bombarded with atomic and molecular noble-gas ions. Surf. Sci. 90, 557-563.

Yasuda H, Sekiguchi T. (1979). Computational studies on ionization processes of laser-produced high-Z plasmas. Jap. J. Appl. Phys. 18, 12:2245-2254.

Discussion with Reviewers

W. Husinsky: My first and strongest criticism concerns the terminology "laser ionization processes in mass spectrometry" (used throughout the entire paper), which according to my opinion seems to be misleading or at least confusing in many cases. Particularly, used together with mass spectrometry laser ionization is commonly used for ionizing free atoms as, for instance, in SNMS. Would not "laser desorption" or "laser sputtering" be expressions more appropriate in this context?

Authors: The general expression "laser ionization processes in mass spectrometry" is not appropriate indeed, since - if the light source is a laser - it covers photoionization experiments as well. In the paper we tried to avoid this ambiguity in two ways. We emphasized from the title on, that the work is confined to microprobing, i.e., investigation of solid targets on a microscopic scale. The other restriction we made - partly inspired by the reviewer - was to use "laser ionization mass spectrometry of solids" instead of simply "laser ionization mass spectrometry". The terms "laser desorption" or "laser sputtering" suggested by the reviewer are not general enough, since they name only particular processes involved in the laser - solid target interaction.

J. D. Brown: According to my view Eq. (2) appears to be incorrect. Shouldn't it read:

$$\Phi(x,t) \;=\; \Phi_0 \int_0^\infty exp[-\alpha(x,t)]dx \quad ?$$

Authors: Integration of our Eq. (1) truncated to the first term on right hand side and considering $\Phi(x = +\infty, t) = \Phi_0(t)$, i.e., that the light comes from $x > 0$, yields our Eq. (2) (see also Mulser, 1970).

W. Husinsky: I miss the discussion of one important (as I see it) question never mentioned in the context: How far does the wavelength of the laser radiation influence the whole story? It has been shown in many desorption experiments that totally different mechanisms might be important for different wavelengths, ranging from thermal to electronic bond-breaking mechanisms.

Authors: In the context of our model there are two places where the wavelength dependence might enter: these are the two terms of Eq. (23). The normal absorption of the solid, α_0, and the plasma absorption, characterized by α_{pl}, are both wavelength dependent. α_0 is strongly varying with the wavelength exhibiting large values at photon energies corresponding to transition energies of internal excitations. Typically in UV electronic excitations and interband transitions occur, while in IR bond vibrations and phonon excitations are responsible for the normal absorption of solid targets. Since during the investigation described in the paper we used $\alpha_0 = 10^{-19} n_n$ and the number density of the solid was $n_n = 10^{22} cm^{-3}$ the normal absorption reached $\alpha_0 = 1000 cm^{-1}$ corresponding to a moderately opaque target. The wavelength dependence of the plasma absorption is fully described by Eq. (24), so the effect of changing the wavelength, i.e. using different lasers can be examined by changing the normal absorption coefficient. Since the submission of the manuscript we have carried out calculations for CO_2, ruby and frequency quadrupled Nd-YAG lasers in the case of transparent and opaque insulators, semiconductors and metallic targets. These results will be published later.